Mesozoic-Cenozoic cooling history of the Eastern Qinghai Nan Shan (NW China): Apatite low-temperature thermochronology constraints

Xu Lin, Marc Jolivet, Jing Liu-Zeng, Feng Cheng, Yuntao Tian, Chang An Li

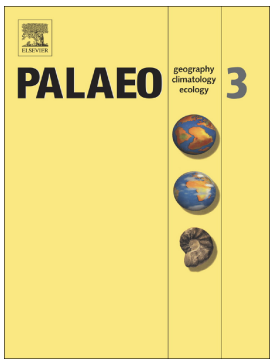

Mesozoic-Cenozoic cooling history of the Eastern Qinghai Nan Shan (NW China): Apatite low-temperature thermochronology constraints

Xu Lin, Marc Jolivet, Jing Liu-Zeng, Feng Cheng, Yuntao Tian, Chang an Li

PII: S0031-0182(21)00201-7

DOI: https://doi.org/10.1016/j.palaeo.2021.110416

Reference: PALAEO 110416

To appear in: *Palaeogeography, Palaeoclimatology, Palaeoecology*

Received date: 20 March 2020

Revised date: 11 March 2021

Accepted date: 13 April 2021

Please cite this article as: X. Lin, M. Jolivet, J. Liu-Zeng, et al., Mesozoic-Cenozoic cooling history of the Eastern Qinghai Nan Shan (NW China): Apatite low-temperature thermochronology constraints, *Palaeogeography, Palaeoclimatology, Palaeoecology* (2018), https://doi.org/10.1016/j.palaeo.2021.110416

Mesozoic-Cenozoic cooling history of the Eastern Qinghai Nan Shan (NW China): apatite low-temperature thermochronology constraints

Xu Lin[a], Marc Jolivet[b], Jing Liu-Zeng[c], Feng Cheng[d], Yuntao Tian[e], Chang'an Li[f]

a. College of Civil Engineering and Architecture, China Three Gorges University, Yichang 443002, China(345837284@qq.com)

b. Laboratoire Géosciences Rennes, CNRS-Université Rennes 1, Observatoire des Sciences de l'Univers de Rennes, Rennes 35042, France(marc.jolivet@univ-rennes1.fr)

c. Institute of Surface-Earth System Science, Tianjin University, Tianjin 300072, China (liu_zeng@tju.edu.cn)

d. Department of Earth and Environmental Science, University of Rochester, Rochester, NY 14627, USA(cfcf.chengfeng@gmail.com)

e. School of Earth Sciences and Engineering, Sun Yat-sen University, Guangzhou 510275, China(tianyuntao@mail.sysu.edu.cn)

f. School of Earth Sciences, China University of Geosciences, Wuhan 430074, China (1002858465@qq.com)

Abstract: Understanding the formation of the Qilian Shan in the NE Tibetan Plateau provides insights into the growth mechanisms of the northern portion of the plateau through time. The onset time of exhumation in the Qilian Shan is still debated. The Qinghai Nan Shan subrange, located in the southeastern Qilian Shan, is cut by the Yellow River that forms Longyang Gorge, providing a good vertical profile for thermochronological investigation of exhumation. In this paper, we reconstruct the

cooling and exhumation history of the Eastern Qinghai Nan Shan using apatite fission-track(AFT) and apatite (U-Th)/He(AHe) thermochronological dating on basement rocks. The fission-track data display a marked age-elevation trend from Early Cretaceous (114-122 Ma) ages at the bottom of the canyon to Early-Middle Jurassic ages (165-180 Ma) at the top. Mean (U-Th)/He ages are mainly Early Cretaceous (97-128 Ma) with one Eocene outlier (42 Ma). Combined with fission track lengths, D_{par} values and thermal modeling results, these data indicate that the study area resided above the closure temperature of AFT and AHe until Early Cretaceous. Rapid cooling occurred during the Early Cretaceous and early Cenozoic likely driven by the Lhasa and Indian blocks collision with the southern margin of the Asian continent. Nonetheless, since then exhumation was limited to less than a few kilometers in the study area. Combined with regional geological studies, the thermochronological analysis demonstrates that, since the Mesozoic, intense exhumation occurred simultaneously along the northern and southern margins of the Qilian Shan. Hence, we suggest that the geomorphic framework of the northeast margin of the Tibetan Plateau was established during the Early Cretaceous-early Cenozoic.

Key words: Tibetan Plateau, Longyang Gorge, Yellow River, Fission track, U-Th/He

1. Introduction

The uplift of the Tibetan Plateau is one of the important geological event in East Asia (Fig. 1a), which had a profound impact on the regional and global climatic change (An et

al., 2001; Guo et al., 2002; Molnar, 2005; Sun et al., 2015; Ding et al., 2017), geomorphic evolution (Brookfield, 1998; Jolivet et al., 2001; Liu-Zeng et al., 2008; Wang et al., 2008; Zheng et al., 2013; Meng et al., 2020), and animal and plant evolution (Deng et al., 2012; Spicer et al., 2020). However, how and when the Tibetan Plateau reached its modern extent is still debated. The Qilian Shan ("shan" = mountains) is a NW-SE trending orogenic belt on the northeastern margin of the Tibetan Plateau (Fig. 1b), which is an ideal area to study the exhumation and expansion mode of the Tibetan Plateau (Yin and Harrison, 2000; George et al., 2001; Song et al., 2001; Jolivet et al., 2001; Zheng et al., 2010; Lin et al., 2011; Xiao et al., 2012; Pan et al., 2013; Wang et al., 2017a; An et al., 2018; Shi et al., 2018; Yu et al., 2019a,b; Tong et al., 2020). The range has a long and complex tectonic history, including late Proterozoic-early Paleozoic oceanic sutures and associated continental collision events as well as several late Paleozoic, Mesozoic and Cenozoic intracontinental deformation events (Yin and Harrison, 2000; Yang et al., 2001; Xu et al., 2006; Xiao et al., 2009; Song et al., 2013; Zuza et al., 2018; Cheng et al., 2019a; Lin et al., 2019; Li et al., 2020a). Even though the geological history of the range has been largely studied, the timing of the Mesozoic and Cenozoic deformation phases and the resulting uplift and exhumation are still controversial. Several studies concluded that the Qilian Shan experienced strong uplift during the Mesozoic (Vincent and Allen,1999; Ritts and Biffi, 2000; Jolivet et al., 2001; Horton et al., 2004; Lin et al., 2011; Jian et al., 2018; Zuza et al., 2018; Cheng et al., 2019a,d). As for the Cenozoic, some studies propose that the deformation initiated at roughly the same time as the initial India-Asia collision (Yin et al., 2002; Dai et al., 2006; Guo et al., 2009; Cheng X et al., 2016; Wang

et al., 2016a; Cheng et al., 2019b; Fang et al., 2019; Zuza et al., 2019). However, others suggested that uplift initiated much more recently, in the late Cenozoic (Tapponnier et al., 2001; Lease et al., 2011; Zhang et al., 2012; Wang et al., 2016b; Hu et al., 2019). Similarly, the models proposed for the uplift pattern of the Qilian Shan imply either stepwise uplift from south to north (Zheng et al., 2017; Zhuang et al., 2018; Cheng et al., 2019b) or synchronous uplift from both north and south (Jolivet et al., 2001; He et al., 2017, 2018; Zuza et al., 2018; Cheng et al., 2019c).

The eastern part of the Qilian Shan is drained by the Yellow River, which is the largest exorheic river in the northeastern Tibetan Plateau. It flows out of the eastern section of the Qilian Shan, cutting a series of deep canyons such as the Longyang Gorge located in the Eastern Qinghai Nan Shan (Perrineau et al., 2011; Nie et al., 2015; Su et al., 2020). There, the Yellow River has incised more than 2 km below a low-relief regional surface (Liu-Zeng et al., 2008). Low-temperature thermochronological studies on vertical profiles along deeply incised river valleys have proven an effective approach to decipher the exhumation time and rates in orogenic belts such as the Longmen Shan, along the eastern margin of the Tibetan Plateau (Kirby et al., 2002; Clark et al., 2005; Jolivet et al., 2015; Tian et al., 2015; Zhang et al., 2016; Liu-Zeng et al., 2018). Apatite (U-Th)/He (AHe) (application range of 40 °C to 80 °C, representing the helium partial retention zone (HePRZ)) (Ehlers and Farley, 2003) and apatite fission track (AFT) (application range of ~110±10 °C to 60 °C, defining the Partial Annealing Zone (PAZ)) (Donelick et al., 2005) thermochronology has already been used to describe the evolution of the Qilian Shan (Jolivet et al., 2001; Wang et al., 2004; Lin et al., 2011; Pan et al., 2013; Li et al., 2019;

Wang et al., 2020). The scale of incision along the Longyang Gorge is large enough for low-temperature thermochronology to be used to constrain the long-term rock cooling histories. However, none of these above studies addressed the timing of exhumation using the vertical profiles provided by deeply incised river valleys along the Qilian Shan. Therefore, in this study, we use AFT and AHe data from a sub-vertical profile within the Longyang Gorge to date the exhumation of the range (Fig. 1c). Combining these data with regional geological studies, we discuss the Mesozoic and Cenozoic exhumation history of the Qilian Shan. The results improve our understanding of the tectonic evolution model of the northeast margin of the Tibetan Plateau.

2. Geological and geomorphic settings

The northeastern Tibetan Plateau is bounded by the West Qinling and East Kunlun Shan to the south, the Qilian Shan to the northwest, and the Liupan Shan to the east (Fig. 1a). Among these ranges, the Qilian Shan forms a major NW-trending thrust-fold belt overprinting a system that originally formed during the early Paleozoic and was later reactivated during the Mesozoic and Cenozoic (Xiao et al., 2009; Song et al., 2013; Zuza et al., 2018). The ~300-km-wide and 3000- to 4500-m-high range is one of the most active thrust belts in the India-Asia collision zone (Cheng et al., 2015; Zuza et al., 2016), flanked by basins with a mean elevation of 1500-3000 m. It can be subdivided, from north to south into the North Qilian Shan, the Tuole Shan, the Danghe Nan Shan, the Shule Nan Shan, the Central Qilian Shan, the South Qilian Shan and Zongwulong Shan, the Qinghai Nan Shan and finally the Laji Shan (Xiao et al., 2009, Fig. 1b).

The lithospheric deformation of the northeastern Tibetan Plateau has been governed by convergence and collision of plates in the southern part of the Asian continent (Yin and Harrison, 2000; Zuza et al., 2018; Guillot et al., 2019, Fig. 1a). During the Jurassic and Cretaceous, the northeastern Tibetan Plateau has been affected by compressive tectonic deformation (Qinghai Geologic Bureau, 1989; Ritts and Biffi, 2000), as suggested by several angular unconformities in the Jurassic-Cretaceous coarse-grained clastic deposits of the Qaidam Basin to the south, the Hexi Corridor to the north and the Xining Basin to the east (Qinghai Geologic Bureau, 1989; Vincent and Allen, 1999; Horton et al., 2004). The Cenozoic tectonic evolution of the Qilian Shan was characterized by a renewed and intense episode of tectonic uplift driven by the ongoing India-Eurasia convergence and the associated rise, thickening, shortening and lateral extrusion of the Tibetan Plateau (Jolivet et al., 1999; Yin and Harrison, 2000; Wu et al., 2012; Cheng et al., 2016; Zuza et al., 2018).

The Qinghai Nan Shan is separating the Gonghe Basin to the south from the Qinghai Lake to the north (Chang et al., 2009; Fu et al., 2013, Fig. 2). The sub-range connects with the Zongwulong Shan to the west and the Laji Shan to the east, forming the southern rim of the Qilian Shan. Paleozoic and Mesozoic basic volcanic rocks, coarse-grained granodiorite and granites were intruded into the basement of the Qinghai Nan Shan (Qinghai Geologic Bureau, 1989, Fig. 2). Resting unconformably on the basement, Triassic, Jurassic and Neogene sedimentary rocks are widely distributed.

The Yellow River flows out of the eastern part of the Gonghe Basin and cuts through the Qinghai Nan Shan to form the Longyang Gorge. It is a 33 km long, 9 km wide and

900 m deep canyon (Fig. 3). Lake spillover in the Gonghe Basin and/or fluvial headwater erosion in the Guide Basin formed the deep Longyang Gorge during the period 1.2-0.012 Ma (Craddock, 2011; Zhang et al., 2014; Guo et al., 2018). A series of stepped erosion surfaces are exposed north and south of the gorges, the upper and most extended one being covered by flat lying Neogene to Quaternary sediments (Fang et al., 2005, Fig. 3). To the north, the base of the sediment cover is represented by Early Miocene alluvial fans of the Garang and Guide formations resting unconformably on the major surface worn through a basement formed by early Mesozoic granites and Triassic sediments (Fang et al., 2005). These deposits are overlain by the Late Miocene-Early Pliocene alluvial and lacustrine Ashigong and Herjia formations (Fang et al., 2005). The whole series are capped by Quaternary lacustrine and aeolian deposits (Guo et al., 2018). To the south, the Early Miocene deposits seem to be lacking and Late Miocene sediments directly cover the erosion surface.

3. Sampling and method

3.1 Sampling strategy

The vertical profile approach uses samples collected over significant relief and a short horizontal distance in order to reconstruct the exhumation history of the region (Fitzgerald et al., 1999; Braun, 2002). We collected seven granite samples from an altitudinal transect (36°17′25″N-36°07'30"N, 100°51′16″E-100°59'30"E) that maximizes relief by spanning the high elevation (3270 m), low-relief surfaces (2350 m), to near the Longyang Gorge bottom on the southern flanks of the Eastern Qinghai Nan Shan (Fig. 3;

Table 1). One additional bedrock sample (HR-9) was collected from bank of the Langma River (a tributary of the Yellow River, 36°08′29″N, 101°02′19″E, 2537 m) on the northern piedmont of the studied area. Samples cover an elevation range from 2350 m to 3270 m, measured using a hand-held Garmin GPS receiver. An age-elevation profile where AFT and/or AHe ages are plotted versus sample elevation allows for the evaluation of variations in the apparent exhumation rate (Fitzgerald et al., 1999; Braun, 2002). In this case, the elevation difference between the two samples (uppermost sample:h_1 and lowermost sample:h_2) is divided by the corresponding sample ages difference (uppermost sample:t_1 and lowermost sample:t_2) to obtain the exhumation rate, E: $E=(t_1-t_2)/(h_1/h_2)$ (Blythe et al., 2007; Malusà and Fitzgerald, 2019).

3.2 Analytical methods

Basement rock samples were crushed mechanically. Apatite grains were concentrated following standard procedures using heavy liquid and magnetic separation techniques. AFT analyses were performed at the Chronus Camp Research, Brazil. Apatite grains were mounted in epoxy resin, cut to expose internal grain surfaces. Sample mounts were etched in 5.5 M HNO_3 at 21 °C for 20 s to reveal the spontaneous fission tracks (Carslon et al., 1999). Spontaneous fission tracks were counted using a Zeiss microscope with a magnification of 1000. The lengths of horizontal confined tracks were measured in order to construct an AFT length-frequency distribution and model the thermal history of the samples. AFT ages were obtained using direct measurements of uranium concentrations with a Neptune high-resolution multi-collector ICP-MS coupled with a

193 Analyte Excite laser ablation system. The detailed dating method can be found in Soares et al. (2015). The uranium concentration of each counted grain was determined using a laser ablation spot size covering the maximum area over which etched tracks had been previously counted. The size of the area for fission-track measurement and consequently the LA-ICP-MS laser ablation depends on the grain size and the occurrence of inclusions or fractures with the standard analyzes beam size between 30-40 μm. The NIST SRM 610 standard was used as an independent check on LA-ICP-MS system performance. AFT ages were calculated using the scheme described by Donelick et al. (2005) based on an adaptation of the zeta calibration approach of Hurford and Green (1983) and Hasabe et al. (2004). The chemical composition of the apatite affects the characteristics of the annealing process, and the D_{par} parameter was used as a proxy for the annealing kinematics (Donelick et al., 2005; Sobel and Seward, 2010). The horizontal confined fission tracks were measured on surfaces parallel to the crystal C-axis (Green et al., 1986). For samples that passed the χ^2 test with age dispersion **<** 10%, the pooled ages are used. However, due to the large spread of single grain ages (Gleadow et al., 1986; An et al., 2020; Li et al., 2020b), or chemical composition variation of apatite grains in a single sample (Galbraith and Laslett, 1993; O'Sullivan and Parrish, 1995), passing the χ^2 test with age dispersion **>** 20%, the central ages are addressed.

The first step for (U-Th)/He dating was to make suitable grains selection. In general, the grains are selected based on their morphology, size, optical clarity, and compositional uniformity. Thereafter, the euhedral crystals or grains with morphologies that can be geometrically approximated are used as they allow the correction for alpha-ejection

(Flowers, 2009). The AHe analysis was also conducted at Chronus Camp Research, Brazil. Helium concentration was measured using an Alphachron (Australian Scientific Instrument Pty Limited-ASI) mass spectrometer with an extraction temperature of 850-900 °C obtained using a 970 nm diode laser and a heating duration of 5 min. Extraction values of >99% of ^{4}He in the heated crystal were obtained. This was verified through a replicate heating procedure checking that secondary extraction did not account for more than a hot blank. For apatite, 25 μL spike solution (diluted in 7 Mol/L HNO_3) containing about 15 ng/mL U and 5 ng/mL Th ($^{235}U/^{238}U$ = 838±7, $^{230}Th/^{232}Th$ = 10.45±0.05) was added into each vial. The time for full dissolution was about 4h at room temperature. 325 μL reagent grade Milli-Q water was then added to the vial, reaching a total volume of 350 μL. Durango apatite was used as an age standard to verify the quality of the analytical procedure.

The weighted mean AHe ages were calculated using Isoplot/Ex_ver3 (Ludwig, 2003). Accurate interpretation of AHe ages must incorporate the effect of crystal size (radius, Rs) and effective U concentration (eU=U+0.235×Th) as both parameters have a non-negligible effect on the He diffusion (Reiners and Farley, 2001; Farley, 2002; Shuster et al., 2006).

3.3 Thermal modeling

Forward and inverse thermal modeling can be performed simultaneously using the HeFTy software (version 1.9.1) (Ketcham, 2005). Forward modeling is the process of predicting what thermochronometer measurements one would expect for a sample that

has undergone a particular temperature history. A comparison between predicted results and measured values is possible. Inverse models have the distinct advantage over forward modeling by hand of permitting many thousands of forward models to be calculated for a sample, obtaining hundreds or even thousands of acceptable time-temperature histories. A combination of AFT age, confined track length data, and available geological background are considered in the inversion modeling with the following time-temperature path constraints. (a) The maximum time and maximum temperature were set at 270 Ma-160 Ma and 200 °C-160 °C respectively, a temperature above which fission tracks in apatite grains are totally annealed. (b) We assumed an average annual surface temperature of 20 °C. The Kolmogorov-Smirnov test was employed to assess the fit between the modeled and measured track-length distributions, with merit values of 0.5 and 0.05 for good and acceptable fits respectively. Ten thousand paths were calculated for each sample, producing several hundreds of acceptable and good time-temperature paths. To better constrain the low-temperature thermal history of the eastern Qinghai Nan Shan, the time-temperature histories were further modeled using the AHe data and the diffusion model proposed by Farley (2000). The following parameters were used as input: the weighted mean of all measured ages, the grain radius, and the content of uranium, thorium and samarium. Because of intrasample age variability, AHe data had to be entered selectively into the models to achieve reasonable results (Ketcham et al., 2018). Thermal history modeling was carried out for samples with similar or consistent AHe ages. Otherwise, if the AHe ages in the sample were too dispersed, it could not be selected.

4. Results

Six samples from the hanging wall of the Eastern Qinghai Nan Shan thrust fault provided AFT ages and seven samples yielded AHe ages. AFT ages range between 180±11 Ma and 114.3±7.9 Ma. These samples yield fairly consistent mean AHe ages from the vertical section clustering in the Early Cretaceous (128±5.9-97.7±1.6 Ma) and Eocene (42.5±0.6 Ma). Geographic locations and AFT ages with 1σ standard errors are reported in Figure 3 and 5 and Table 2. U, Th, and He concentrations, crystal dimensions, AHe raw and corrected ages are summarized in Table 3.

The AFT age data display a marked correlation with sample elevation (r^2=0.67) allowing to calculate a mean exhumation rate of 15.0 m/Ma ranging from 119 Ma to 180 Ma (Fig. 5). AFT age-elevation profiles from both this and earlier studies in the central part of Qinghai Nan Shan (Craddock, 2011) are presented in Figure 5. These AFT ages are clearly younger than the Indosinian crystallization age(~270Ma) of the granitic intrusions they belong to (Zeng et al., 2018), suggesting post-crystallization cooling through the apatite fission track PAZ during regional exhumation events. The mean track lengths are within 11.9-13.2 μm (Table 2), with standard deviations of 1.53 μm to 2.55 μm. The track length distributions are of "undisturbed basement" type (Gleadow et al., 1986). The D_{par} values vary from 1.0 μm to 4.2 μm and do not show clear relationships with the corresponding AFT ages and fission track lengths implying that chemical heterogeneity of the samples has little effect on the annealing kinetics (Fig. 6).

Three to five single-grain AHe age analyses were performed for each sample from the Longyang Gorge and Langma River transects (Fig. 5). The samples yield single AHe ages ranging from 159.1±7.3 Ma to 36.6±0.5 Ma (Table 3). Most AHe ages are

significantly younger than the AFT ages on the same sample, especially the higher elevation samples (HR-6, HR-7, Fig. 5). The lower elevation samples (LY-1, 2, 3), however, have several single-grain AHe ages that overlap with the AFT ages within uncertainty. In addition, there are some single-grain AHe ages in each of the three lower samples older than their corresponding AFT ages. The comparisons between single-grain AHe ages and eU and Rs do not show clear relationship, suggesting that radiation damages or grain size are not the main factors explaining the abnormally older AHe ages (Shuster et al., 2006, Fig. 7). In contrast, it is likely linked to other magnified factors such as a protracted residence in the apatite (U-Th)/He PRZ (Fitzgerald et al., 2006; Biswas et al., 2007; Clinkscales et al., 2020), U, and Th zoning (Flowers and Kelley, 2011) or other elements zoning (Jolivet et al., 2003; Djimbi et al., 2015).

Modeled t-T paths obtained from AFT data are shown in Figure 8. Samples HR-6, and HR-7 cooled relatively rapidly during the Middle Triassic to the Early-Middle Jurassic, before a phase of slow cooling through the PAZ, which the samples exited during the Early Cretaceous (HR-7) to Late Cretaceous (HR-6). Samples LY-1, LY-2 and LY-3 are characterized by a poorly defined initial cooling during the Triassic to Jurassic up to the base of the PAZ followed by a rapid cooling that initiated during the Early Cretaceous. Modeling of AHe data confirm the occurrence of a Cretaceous-early Cenozoic exhumation event (Fig. 9).

5. Discussion

5.1 Exhumation history of the Eastern Qinghai Nan Shan and implications for the

formation of the Qilian Shan

AFT ages of samples HR-6 and HR-7 at the top of the Eastern Qinghai Nan Shan cluster at 180±11-165±9.5 Ma, cooling below the AFT PAZ occurred during the Early-Middle Jurassic. AFT and AHe thermal history modeling results and AHe ages from the lower samples LY-1 and LY-2 also support a Jurassic cooling in the Eastern Qinghai Nan Shan. Regionally, Jurassic cooling has been reported from the North Qilian Shan (George et al., 2001; Jolivet et al., 2001; Li et al., 2019), the Altun Shan (Sobel et al., 2001), the East Kunlun Shan (Tian et al., 2020), the Liupan Shan (Lin et al., 2011; Peng et al., 2019), the West Qinling Shan (Zattin and Wang, 2019) or the Longmen Shan (Roger et al., 2010; Jolivet et al., 2015). Jurassic cooling event may be the response to the collision between the Qiangtang and Kunlun blocks (Jolivet et al., 2001; Karplus et al., 2011; Tian et al., 2020; Zhang et al., 2020a).

However, on the age-elevation profile, the bottom three samples (LY-1, LY-2, and LY-3) show overlapping mean AFT and AHe ages concentrated in the Early Cretaceous (Fig. 5), which suggests the Eastern Qinghai Nan Shan experienced rapid exhumation during that time. This timing is further confirmed by the AFT and AHe thermal history modeling results. Similar events have been suggested based on AFT and AHe ages in the central part of Qinghai Nan Shan (Craddock, 2011, Fig. 5). In addition, Craddock (2011)'s AHe results support a rapid exhumation during the early Cenozoic (39-51 Ma), consistent with the AHe age in sample HR-9 (42 Ma) obtained in this study. Such an outlier AHe age (HR-9) is likely to be controlled by regional fault activity. Therefore, it indicates that exhumation again appeared in the whole Qinghai Nan Shan during the early

Cenozoic. However, that amount of Cenozoic exhumation was probably not large enough to completely erase the Mesozoic low temperature signal still preserved in the range.

Moreover, tectonic exhumation events can also be found in the Central and North Qilian Shan during the Early Cretaceous and Early Cenozoic. For example, bedrock apatite FT age and thermal history modeling results show that the Central Qilian Shan were exhumed rapidly at 120-68 Ma and 60-40 Ma (Qi et al., 2016; He et al., 2020, Fig. 10), which is consistent with the detrital AFT ages from the adjacent sedimentary strata (Li et al., 2020b). Similarly, bedrock and detrital AFT ages indicate that intense exhumation occurred in the North Qilian Shan at 115-80 Ma (George et al., 2001; Jolivet et al., 2001; Duvall et al., 2013; Bao et al., 2013; Lin et al., 2019) and 59-38 Ma (He et al., 2017; Li et al., 2019, Fig. 10). Sediments characteristics in the northeastern Qaidam Basin and Hexi Corridor provide evidence of simultaneous sustained exhumation in the South and North Qilian Shan during the Early Cretaceous and early Cenozoic (Vincent and Allen, 1999; Ritts and Biffi, 2000; Dai et al., 2005; Fang et al., 2005; Yin et al., 2008a,b; Cheng et al., 2019b,d; Zhang et al., 2020b). It is therefore that both the Early Cretaceous and the early Cenozoic are the most important periods for the formation of the Qilian Shan.

5.2 Implications for intracontinental deformation of the northeastern Tibetan Plateau

Combined with existing low-temperature thermochronology datasets and thermal history modeling results, we infer that the intense exhumation occurred in the whole

Qinghai Nan Shan during the Early Cretaceous and early Cenozoic. However, thick Early Miocene sandstone and conglomerate deposits (Garang and Guidemen fms.) are widely distributed in the piedmonts of the Eastern Qinghai Nan Shan, unconformably overlying the crystalline basement (Fig. 3). Moreover, well-developed Late Miocene initiated growth strata along the western and central parts of Qinghai Nan Shan, revealed that strong topographic gradients occurred in the Late Miocene-Pliocene (Chang et al., 2009; Zhang et al., 2012). Our low temperature thermochronology data and thermal modeling results, however, do not show any Neogene cooling event. Considering the mean exhumation rate derived from our models (15.0 m/Ma), the total exhumation of the Eastern Qinghai Nan Shan at 120 Ma can reach ~300 m while the subsequent exhumation is very limited. Regional exhumation in the study area and central parts of Qinghai Nan Shan during the Neogene (Craddock, 2011) was not enough to completely obliterate the Mesozoic signal. Although the Qinghai Nan Shan underwent rapid exhumation during the Early Cretaceous and early Cenozoic, the subsequent exhumation was limited and the Miocene intense exhumation occurred (Chang et al., 2009; Craddock, 2011; Zhang et al., 2012), most probably due to tectonic compression. A similar orogenic belt exhumation pattern was discussed in the West Qinling Shan (Zattin and Wang, 2019) and eastern part of the North Qilian Shan (Pan et al., 2013; Li et al., 2019).

Regionally, Early Cretaceous-early Cenozoic exhumation events are also recorded in the Liupan Shan (Lin et al., 2011; Peng et al., 2019), the Altun Shan (Jolivet et al., 2001; Sobel et al., 2001), the Qimantagh Shan (Wang et al., 2019), the East Kunlun Shan (Yuan et al., 2006; Dai et al., 2013; Wang et al., 2017c), as well as in the Kuantan Shan and

Longshou Shan (Zhang et al., 2017; An et al., 2020). We suggest that the geomorphic framework of the northeast margin of the Tibetan Plateau was initially established during the Early Cretaceous in response to the collision of the Qiangtang and Lhasa blocks (120 Ma, Kapp et al., 2007; Guillot et al., 2019; Zhang et al., 2019) and further enhanced during the early Cenozoic initial stage of the Indian collision (Hu et al., 2016).

6. Conclusions

New AFT and AHe thromochronological data combined with inverse thermal modeling from the Eastern Qinghai Nan Shan record exhumation during the Early Cretaceous-early Cenozoic following a period of continuous but slow cooling during the Late Jurassic. We relate this first exhumation phase to the collision between the Qiangtang and the Kunlun blocks, and the second exhumation to the collisions of the Lhasa and Indian blocks with the southern margin of Eurasia. However, the Early Cretaceous-early Cenozoic exhumation was not sufficient to completely exhume the early Mesozoic apatite PAZ as Early Jurassic AFT ages are still preserved. Combined with previous regional geological studies, indicates intense exhumation occurred simultaneously along the northern and southern margins of the Qilian Shan since the Mesozoic. The geomorphic framework of the northeast margin of the Tibetan Plateau was initially established since the Early Cretaceous.

Acknowledgements

We wish to thank Xitao Zhao from the Institute of Geology and Geophysics at Chinese

Academy of Sciences in Beijing for helping us so much with the field work for this study. This work was financially supported by the National Natural Science Foundation of China (Grant 41671011, 41702178, 41972212), and the Hunan Natural Science Foundation of China (Grant 2019JJ40198). Profound comments and suggestions from the Guest editor Dr. Ryan Leary, Reviewer Dr. Xiubin Lin, Dr. Devon Orme and an anonymous reviewer are appreciated, which help to improve the paper significantly.

References

An, Zh., Kutzbach, E., Prell, L., Porter, C., 2001. Evolution of Asian monsoons and phased uplift of the Himalaya-Tibetan plateau since Late Miocene times. Nature, 411, 62-66.

An, K., Lin, X., Wu, L., Cheng, X., Chen, H., Ding, W., Li, C. 2018. Reorganization of sediment dispersal in the Jiuxi Basin at ~17 Ma and its implications for uplift of the Tibetan Plateau. Palaeogeography, Palaeoclimatology, Palaeoecology, 511, 558-576.

An, K., Lin, X., Wu, L., Yang, R., Chen, H., Cheng, X., Li, C. 2020. An immediate response to the Indian-Eurasian collision along the northeastern Tibetan Plateau: Evidence from apatite fission track analysis in the Kuantan Shan-Hei Shan. Tectonophysics, 774, 228278.

Biswas, S., Coutand, I., Grujic, D., Hager, C., Stöckli, D., Grasemann, B. 2007. Exhumation and uplift of the Shillong plateau and its influence on the eastern Himalayas: New constraints from apatite and zircon (U-Th-[Sm])/He and apatite fission track analyses. Tectonics, 26(6), 1-22.

Blythe, A. E., Burbank, D. W., Carter, A., Schmidt, K., Putkonen, J. 2007.

Plio-Quaternary exhumation history of the central Nepalese Himalaya: 1. Apatite and zircon fission track and apatite [U-Th]/He analyses. Tectonics, 26(3), 1-16.

Braun, J. 2002. Estimating exhumation rate and relief evolution by spectral analysis of age–elevation datasets. Terra Nova, 14(3), 210-214.

Brookfield, M. E. 1998. The evolution of the great river systems of southern Asia during the Cenozoic India-Asia collision: rivers draining southwards. Geomorphology, 22(3-4), 285-312.

Carlson, W.D., Donelick, R.A., Ketcham, R.A., 1999. Variability of apatite fission-track annealing kinetics: I. Experimental results. Am. Mineral, 84, 1213-1223.

Clark, M. K., M. A. House, L. H. Royden, K. X. Whipple, B. C. Burchfiel, X. Zhang, and W. Tang. 2005. Late Cenozoic uplift of southeastern Tibet. Geology, 33(6), 525–528.

Clinkscales, C., Kapp, P., Wang, H. 2020. Exhumation history of the north-central Shanxi Rift, North China, revealed by low-temperature thermochronology. Earth and Planetary Science Letters, 536, 116146.

China Geological Survey. 2004. 1:2.5 million scale geologic map of China. Sino Maps Press, Beijing, 1.

Chang, H., Jin, Z., An, Z. 2009. Sedimentary evidence of the uplift of the Qinghai Nanshan (the Mountains south to Qinghai Lake) and its implication for structural evolution of the lake Qinghai-Gonghe Basin. Geological Review, 55, 49-57(in Chinese with English abstract).

Cheng, F., Jolivet, M., Dupont-Nivet, G., Wang, L., Yu, X., Guo, Z. 2015. Lateral

extrusion along the Altyn Tagh Fault, Qilian Shan (NE Tibet): insight from a 3D crustal budget. Terra Nova, 27(6), 416-425.

Cheng, F., Jolivet, M., Fu, S., Zhang, C., Zhang, Q., Guo, Z. 2016. Large-scale displacement along the Altyn Tagh Fault (North Tibet) since its Eocene initiation: Insight from detrital zircon U-Pb geochronology and subsurface data. Tectonophysics, 677, 261-279.

Cheng, F., Jolivet, M., Guo, Z., Lu, H., Zhang, B., Li, X., Wang, Z. 2019a. Jurassic-Early Cenozoic Tectonic Inversion in the Qilian Shan and Qaidam Basin, North Tibet: New Insight From Seismic Reflection, Isopach Mapping, and Drill Core Data. Journal of Geophysical Research: Solid Earth, 124(11), 12077-12098.

Cheng, F., Garzione, C. N., Mitra, G., Jolivet, M., Guo, Z., Lu, H., Wang, L. 2019b. The interplay between climate and tectonics during the upward and outward growth of the Qilian Shan orogenic wedge, northern Tibetan Plateau. Earth-Science Reviews, 198, 102945.

Cheng, F., Garzione, C., Jolivet, M., Guo, Z., Zhang, D., Zhang, C, Zhang, Q. 2019c. Initial Deformation of the Northern Tibetan Plateau: Insights From Deposition of the Lulehe Formation in the Qaidam Basin. Tectonics, 38, 741-766.

Cheng, F., Garzione, C., Jolivet, M., Wang, W., Dong, J., Richter, F., Guo, Z. 2019d. Provenance analysis of the Yumen Basin and northern Qilian Shan: Implications for the pre-collisional paleogeography in the NE Tibetan Plateau and eastern termination of Altyn Tagh fault. Gondwana Research, 65, 156-171.

Cheng, X., Lin, X., Wu, L., Chen, H., Xiao, An., Gong, J., Yang, Sh., 2016. The Exhumation History of North Qaidam Thrust Belt Constrained by Apatite Fission Track Thermochronology: Implication for the Evolution of the Tibetan Plateau. Acta Geologica Sinica, 90, 870-883.

Craddock, W. H. 2011. Structural and geomorphic evolution of the Gonghe Basin complex, northeastern Tibet: implications for the timing of plateau growth. The Pennsylvania State University, 1-271.

Dai, S., Fang, X., Song, C., Gao, J., Gao, D., Li, J., 2005. Early tectonic uplift of the northern Tibetan Plateau. Chinese Science Bulletin, 50(15), 1642-1652.

Dai, S., Fang, X., Dupont-Nivet, G., Song, C., Gao, J., Krijgsman, W., . Zhang, W. 2006. Magnetostratigraphy of Cenozoic sediments from the Xining Basin: Tectonic implications for the northeastern Tibetan Plateau. Journal of Geophysical Research: Solid Earth, 111,1-19.

Dai, J., Wang, C., Hourigan, J., Santosh, M. 2013. Multi-stage tectono-magmatic events of the Eastern Kunlun Range, northern Tibet: insights from U–Pb geochronology and (U-Th)/He thermochronology. Tectonophysics, 599, 97-106.

Donelick, R.A., O'Sullivan, P.B., Ketcham, R.A., 2005. Apatite Fission-Track Analysis. Reviews in Mineralogy and Geochemistry, 58, 49-94.

Duvall, A.R., Clark, M.K., Kirby, E., Farley, K.A., Craddock, W.H., Li, C., Yuan, D. Y., 2013. Low-temperature thermochronometry along the Kunlun and Haiyuan Faults, NE Tibetan Plateau: Evidence for kinematic change during late-stage orogenesis. Tectonics, 32, 1190-1211.

Ding, L., Spicer, R. A., Yang, J., Xu, Q., Cai, F., Li, S., Shukla, A. 2017. Quantifying the rise of the Himalaya orogen and implications for the South Asian monsoon. Geology, 45(3), 215-218.

Djimbi, D. M., Gautheron, C., Roques, J., Tassan-Got, L., Gerin, C., Simoni, E. 2015. Impact of apatite chemical composition on (U-Th)/He thermochronometry: An atomistic point of view. Geochimica et Cosmochimica Acta, 167, 162-176.

Deng, T., Li, Q., Tseng, Z. J., Takeuchi, G. T., Wang, Y., Xie, G., Wang, X. 2012. Locomotive implication of a Pliocene three-toed horse skeleton from Tibet and its paleo-altimetry significance. Proceedings of the National Academy of Sciences, 109(19), 7374-7378.

Ehlers, T, A., Farley, K, A. 2003. Apatite (U-Th)/He thermochronometry: methods and applications to problems in tectonic and surface processes. Earth Planetary Science Letters, 206, 1-14.

Fang, X., Yan, M., Voo, R. V. D., Rea, D. K., Song, C., Parés, J. M. 2005. Late Cenozoic deformation and uplift of the NE Tibetan Plateau: evidence from high-resolution magnetostratigraphy of the Guide Basin, Qinghai Province, China. Geological Society of America Bulletin, 117, 1208-1225.

Fang, X., Fang, Y., Zan, J., Zhang, W., Song, C., Appel, E. 2019. Cenozoic magnetostratigraphy of the Xining Basin, NE Tibetan Plateau, and its constraints on paleontological, sedimentological and tectonomorphological evolution. Earth-Science Reviews, 190, 460-485.

Farley, K. A. 2000. Helium diffusion from apatite: General behavior as illustrated by

Durango fluorapatite. Journal of Geophysical Research: Solid Earth, 105(B2), 2903-2914.

Farley, K. A. 2002. (U-Th)/He dating: Techniques, calibrations, and applications. Reviews in Mineralogy and Geochemistry, 47(1), 819-844.

Flowers, R, M. 2009. Exploiting radiation damage control on apatite (U-Th)/He dates in cratonic regions. Earth Planetary Science Letters, 277, 148-155.

Flowers, R, M., Kelley, S, A. 2011. Interpreting data dispersion and " inverted " dates in apatite (U-Th)/He and fission-track datasets: An example from the US midcontinent. Geochimica Et Cosmochimica Acta, 75, 5169-5186.

Fitzgerald, P. G., Muñoz, J. A., Coney, P. J., Baldwin, S. L.1999. Asymmetric exhumation across the Pyrenean orogen: implications for the tectonic evolution of a collisional orogen. Earth and Planetary Science Letters, 173(3), 157-170.

Fitzgerald, P. G., Baldwin, S. L., Webb, L. E., O'Sullivan, P. B. 2006. Interpretation of (U-Th)/He single grain ages from slowly cooled crustal terranes: a case study from the Transantarctic Mountains of southern Victoria Land. Chemical Geology, 225(1-2), 91-120.

Fu, C., An, Z., Qiang, X., Bloemendal, J., Song, Y., Chang, H. 2013. Magnetostratigraphic determination of the age of ancient Lake Qinghai, and record of the East Asian monsoon since 4.63 Ma. Geology, 41, 875-878.

Galbraith, R.F., Laslett, G.M., 1993. Statistical models for mixed fission track ages. Nuclear Tracks and Radiation Measurements 21 (4), 459-470.

Green, P.F., Duddy, R., Gleadow, A.J.W., Tingate, P.R., Laslett, G.M., 1986. Thermal

annealing of fission tracks in apatite: 1. A qualitative description. Chemical Geology: Isotope Geoscience section 59, 237-253.

George, A.D., Marshallsea, S.J., Wyrwoll, K. H., Jie, C., Y, L. 2001. Miocene cooling in the northern Qilian Shan, northeastern margin of the Tibetan Plateau, revealed by apatite fission-track and vitrinite-reflectance analysis. Geology, 29, 939-942.

Gleadow, A. J., Duddy, I. R., Green, P. F., Hegarty, K. A. 1986. Fission track lengths in the apatite annealing zone and the interpretation of mixed ages. Earth and planetary science letters, 78(2-3), 245-254.

Guenthner, W. R., Reiners, W., Tian, Y. 2014. Interpreting date-eU correlations in zircon (U-Th)/He datasets: A case study from the Longmen Shan, China. Earth Planetary Science Letters, 403, 328-339.

Guo, Z. T., Ruddiman, W. F., Hao, O. Z., Wu, H. B., Qiao, Y. S., Zhu, R. X., Liu, T. S. 2002. Onset of Asian desertification by 22 Myr ago inferred from loess deposits in China. Nature, 416(6877), 159-163.

Guo, Z., Lu, J., Zhang, Z. 2009. Cenozoic exhumation and thrusting in the northern Qilian Shan, northeastern margin of the Tibetan Plateau: Constraints from sedimentological and apatite fission-track data. Acta Geologica Sinica-English Edition, 83(3), 562-579.

Guo, X., Forman, S. L., Marin, L., Li, X. 2018. Assessing tectonic and climatic controls for Late Quaternary fluvial terraces in Guide, Jianzha, and Xunhua Basins along the Yellow River on the northeastern Tibetan Plateau. Quaternary Science Reviews, 195,

109-121.

Guillot, F. S., Goussin, L., Airaghi, A., Replumaz, J., de Sigoyer, C., Cordier. 2019. How and When Did the Tibetan Plateau Grow? Russian Geology and Geophysics, 60, 957-977.

Hasebe, N., Barbarand, J., Jarvis, K., Carter, A., Hurford, A. J. 2004. Apatite fission-track chronometry using laser ablation ICP-MS. Chemical Geology, 207(3-4), 135-145.

He, P., Song, C., Wang, Y., Chen, L., Chang, P., Wang, Q., Ren, B. 2017. Cenozoic exhumation in the Qilian Shan, northeastern Tibetan Plateau: Evidence from detrital fission-track thermochronology in the Jiuquan Basin. Journal of Geophysical Research: Solid Earth, 122, 6910-6927.

He, P., Song, C., Wang, Y., Meng, Q., Chen, L., Yao, L., Chen, S. 2018. Cenozoic deformation history of the Qilian Shan (northeastern Tibetan Plateau) constrained by detrital apatite fission-track thermochronology in the northeastern Qaidam Basin. Tectonophysics, 719, 1-11.

He, P., Song, C., Wang, Y., Meng, Q., Wang, D., Feng, Y., Feng, W. 2020. Early Cenozoic exhumation in the Qilian Shan, northeastern margin of the Tibetan Plateau: Insights from detrital apatite fission track thermochronology. Terra Nova, in press.

Hurford, A.J., Green, P.F., 1983. The zeta age calibration of fission-track dating. Isot. Geosci. 1, 285-317.

Hu, X., Garzanti, E., Wang, J., Huang, W., An, W., Webb, A. 2016. The timing of India-Asia collision onset–Facts, theories, controversies. Earth-Science Reviews, 160, 264-299.

Hu, X., Chen, D., Pan, B., Chen, J., Zhang, J., Chang, J., Gong, C., Zhao., Q. 2019. Sedimentary evolution of the foreland basin in the NE Tibetan Plateau and the growth of the Qilian Shan since 7 Ma. Geological Society of America Bulletin,131, 1744-1760.

Horton, B., Dupont-Nivet, G., Zhou, J., Waanders, G., Butler, R., Wang, J. 2004. Mesozoic-Cenozoic evolution of the Xining-Minhe and Dangchang basins, northeastern Tibetan Plateau: magnetostratigraphic and biostratigraphic results. J. Geophys. Res. Solid Earth, 109, 1-35.

Jian, X., Guan, P., Zhang, W., Liang, H., Feng, F., Fu, L. 2018. Late Cretaceous to early Eocene deformation in the northern Tibetan Plateau: Detrital apatite fission track evidence from northern Qaidam basin. Gondwana Research, 60, 94-104.

Jolivet, M., Brunel, M., Roger, F., Tapponnier, P., Arnaud, N., Seward, D. 1999. Exhumation history of the Altun Shan with evidence for the timing of the subduction of the Tarim block beneath the Altyn Tagh system, North Tibet. Comptes Rendus de l'Academie des Sciences. Serie 2, Sciences de la Terre et des Planetes, 749-755.

Jolivet, M., Brunel, M., Seward, D., Xu, Z., Yang, J., Roger, F., Tapponnier, P., Malavieille, J., Arnaud, N.W., C. 2001. Mesozoic and Cenozoic tectonics of the northern edge of the Tibetan plateau: fission-track constraints. Tectonophysics 343, 111-134.

Jolivet, M., Brunel, M., Seward, D., Xu, Z., Yang, J., Malavieille, J., Roger, F., Leyreloup, A., Arnaud, N., Wu, C., 2003. Neogene extension and volcanism in the Kunlun Fault Zone, northern Tibet: new constraints on the age of the Kunlun Fault.

Tectonics, 22, 1-23.

Jolivet, M., Roger, F., Xu, Z. Q., Paquette, J. L., Cao, H. 2015. Mesozoic-Cenozoic evolution of the Danba dome (Songpan Garzê, East Tibet) as inferred from LA-ICPMS U-Pb and fission-track data. Journal of Asian Earth Sciences, 102, 180-204.

Kapp, P., DeCelles, P.G., Gehrels, G.E., Heizler, M., Ding, L., 2007. Geological records of the Lhasa-Qiangtang and Indo-Asian collisions in the Nima area of central Tibet. Geological Society of America Bulletin, 119, 917-933.

Ketcham, R. A. 2005. Forward and inverse modeling of low-temperature thermochronometry data. Reviews in mineralogy and geochemistry, 58(1), 275-314.

Ketcham, R. A., Van Der Beek, P., Barbarand, J., Bernet, M., Gautheron, C. 2018. Reproducibility of thermal history reconstruction from apatite fission-track and (U-Th)/He data. Geochemistry, Geophysics, Geosystems, 19(8), 2411-2436.

Karplus, M. S., Zhao, W., Klemperer, S. L., Wu, Z., Mechie, J., Shi, D., Chen, C. 2011. Injection of Tibetan crust beneath the south Qaidam Basin: Evidence from INDEPTH IV wide-angle seismic data. Journal of Geophysical Research: Solid Earth, 116(B7),1-23.

Kirby, E., P. W. Reiners, M. A. Krol, K. X. Whipple, K. V. Hodges, K. A. Farley, W. Q. Tang, and Z. L. Chen. 2002. Late Cenozoic evolution of the eastern margin of the Tibetan Plateau: Inferences from Ar40/Ar39 and (U-Th)/He thermochronology. Tectonics, 21(1), 1001.

Lease, R. O., Burbank, D. W., Clark, M. K., Farley, K. A., Zheng, D., Zhang, H. 2011.

Middle Miocene reorganization of deformation along the northeastern Tibetan Plateau. Geology, 39, 359-362.

Li, B., Chen, X., Zuza, A. V., Hu, D., Ding, W., Huang, P. 2019. Cenozoic cooling history of the North Qilian Shan, northern Tibetan Plateau, and the initiation of the Haiyuan fault: Constraints from apatite-and zircon-fission track thermochronology. Tectonophysics, 751, 109-124.

Li, B., Zuza, A. V., Chen, X., Wang, Z. Z., Shao, Z., Levy, D. A., Sun, Y. 2020a. Pre-cenozoic evolution of the northern Qilian Orogen from zircon geochronology: Framework for early growth of the northern Tibetan Plateau. Palaeogeography, Palaeoclimatology, Palaeoecology, 110091.

Li, B., Zuza, A. V., Chen, X., Hu, D., Shao, Z., Qi, B., Xiong, X. 2020b. Cenozoic multi-phase deformation in the Qilian Shan and out-of-sequence development of the northern Tibetan Plateau. Tectonophysics, 228423.

Lin, X., Chen, H., Wyrwoll, K. H., Batt, G. E., Lin, L., Xiao, J. 2011. The uplift history of the Haiyuan-Liupan Shan region northeast of the present Tibetan Plateau: integrated constraint from stratigraphy and thermochronology. Journal of Geology, 119, 372-393.

Lin, X., Zheng, D., Sun, J., Windley, B.F., Tian, Z., Gong, Z., Jia, Y., 2015. Detrital apatite fission track evidence for provenance change in the Subei Basin and implications for the tectonic uplift of the Danghe Nan Shan (NW China) since the mid-Miocene. Journal of Asian Earth Sciences, 111, 302-311.

Lin, X., Tian, Y., Donelick, R. A., Liu-Zeng, J., Cleber, S. J., Li, C. A., Li, Z. 2019.

Mesozoic and Cenozoic tectonics of the northeastern edge of the Tibetan plateau: Evidence from modern river detrital apatite fission-track age constraints. Journal of Asian Earth Sciences, 170, 84-95.

Liu-Zeng, J., Tapponnier, P., Gaudemer, Y., Ding, L. 2008. Quantifying landscape differences across the Tibetan Plateau: Implications for topographic relief evolution. Journal of Geophysical Research: Earth Surface, 113(4),1-26.

Liu-Zeng, J., Zhang, J., McPhillips, D., Reiners, P., Wang, W., Fik, R., Zheng, D. 2018. Multiple episodes of fast exhumation since Cretaceous in southeast Tibet, revealed by low-temperature thermochronology. Earth and Planetary Science Letters, 490, 62-76.

Ludwig, K. R. 2003. Isoplot 3.00: A geochronological toolkit for Microsoft Excel. Berkeley Geochronology Center Special Publication, 4, 70.

Malusà, M. G., Fitzgerald, P. G. 2019. Application of thermochronology to geologic problems: bedrock and detrital approaches. Springer, Cham: In Fission-Track Thermochronology and its Application to Geology, 191-209.

Meng, K., Wang, E., Chu, J. J., Su, Z., Fan, C. 2020. Late Cenozoic river system reorganization and its origin within the Qilian Shan, NE Tibet. Journal of Structural Geology, 104128.

Molnar, P. 2005. Mio-Pliocene growth of the Tibetan Plateau and evolution of East Asian climate. Palaeontologia Electronica, 8(1), 1-23.

Nie, J., Stevens, T., Rittner, M., Stockli, D., Garzanti, E., Limonta, M. 2015. Loess Plateau storage of Northeastern Tibetan Plateau-derived Yellow River sediment. Nature Communication, 6, 1-8.

Ritts, B.D., Biffi, U. 2000. Magnitude of post-Middle Jurassic (Bajocian) displacement on the central Altyn Tagh fault system, northwest China. Geological Society of America Bulletin 112, 61-74.

Reiners, P. W., Farley, K. A. 2001. Influence of crystal size on apatite (U-Th)/He thermochronology: An example from the Bighorn Mountains, Wyoming. Earth and Planetary Science Letters, 188(3), 413-420.

Roger, F., Jolivet, M., Malavieille, J. 2010. The tectonic evolution of the Songpan-Garzê (North Tibet) and adjacent areas from Proterozoic to Present: A synthesis. Journal of Asian Earth Sciences, 39(4), 254-269.

Song, C., Fang, X., Li, J., Gao, J., Zhao, Z., Fan, M., 2001. Tectonic uplift and sedimentary evolution of the Jiuxi Basin in the northern margin of the Tibetan Plateau since 13 Ma. Science China Series D: Earth Science, 44, 192-202.

Song, S., Cao, D., Zhang, Q., Wang, A., Peng, Y. 2018. Apatite fission track evidence for Miocene denudation history in the Gangdese conglomerate belt and Yarlung Tsangpo River: Implications for the evolution of Southern Tibet. Journal of Asian Earth Sciences, 160, 159-167.

Soares, C. J., Mertz, R., Guedes, S., Stockli, D.F., Zack, T., 2015. Characterization of apatites as potential trace element reference materials for fission-track dating by LAICP-MS. Geostandard Geoanal. Res. 39, 305-313.

Sobel, E.R., Arnaud, N., Jolivet, M., Ritts, B.D., Brunei, M., 2001. Jurassic to Cenozoic exhumation history of the Altyn Tagh range, northwest China, constrained by 40Ar/39Ar and apatite fission track thermochronology. Geol. Soc. Am. Memoir

194, 247-267.

Sobel, E. R., Seward, D. 2010. Influence of etching conditions on apatite fission-track etch pit diameter. Chemical Geology, 271(1-2), 59-69.

Song, S., Niu, Y., Su, L., Xia, X. 2013. Tectonics of the north Qilian orogen, NW China. Gondwana Research, 23, 1378-1401.

Su, Q., Kirby, E., Ren, Z., Zhang, P., Zhang, H., Manopkawee, P., Lei, Q. 2020. Chronology of the Yellow River terraces at Qingtong Gorge (NE Tibet): Insights into evolution of the Yellow River since the Middle Pleistocene. Geomorphology, 349, 106889.

Sun, J., Gong, Z., Tian, Z., Jia, Y., Windley, B. 2015. Late Miocene stepwise aridification in the Asian interior and the interplay between tectonics and climate. Palaeogeography, Palaeoclimatology, Palaeoecology, 421, 48-59.

Shi, W., Wang, F., Yang, L., Wu, L., Zhang, W. 2018. Diachronous growth of the Altyn Tagh Mountains: Constraints on propagation of the northern Tibetan margin from (U-Th)/He dating. Journal of Geophysical Research: Solid Earth, 123, 6000-6018.

Shuster, D. L., Flowers, R. M., Farley, K. A. 2006. The influence of natural radiation damage on helium diffusion kinetics in apatite. Earth and Planetary Science Letters, 249(3), 148-161.

Shuster, D.L., Farley, K.A., 2009. The influence of artificial radiation damage and thermal annealing on helium diffusion kinetics in apatite. Geochim. Cosmochim. Acta, 73, 183-196.

Spicer, R. A., Farnsworth, A., Su, T. 2020. Cenozoic Topography, Monsoons and

Biodiversity Conservation within the Tibetan Region: An Evolving Story. Plant Diversity, in press.

Tapponnier, P., Zhiqin, X., Roger, F., Meyer, B., Arnaud, N., Wittlinger, G., Jingsui, Y., 2001. Oblique Stepwise Rise and Growth of the Tibet Plateau. Science, 294, 1671-1677.

Tian, Y., Kohn, B. P., Hu, S., Gleadow, A. J. W. 2014. Postorogenic rigid behavior of the eastern Songpan-Ganze terrane: insights from low-temperature thermochronology and implications for intracontinental deformation in central Asia. Geochemistry Geophysics Geosystems, 15, 453-474.

Tian, Y., Kohn, B. P., Hu, S., Gleadow, A. J. W. 2015. Synchronous fluvial response to surface uplift in the eastern Tibetan Plateau: implications for crustal dynamics. Geophysical Research Letters, 42, 29-35.

Tian, P., Yuan, W., Yang, X., Feng, Z., Chen, X., Yuan, E. 2020. Multi-stage tectonic events of the Eastern Kunlun Mountains, Northern Tibetan Plateau constrained by fission track thermochronology. Journal of Asian Earth Sciences, 104428.

Tong, K., Li, Z., Zhu, T., Tao, G., Zhang, Y., Yang, W., Zhang, J. 2020. Fold-and-thrust deformation of the hinterland of Qilian Shan, northeastern Tibetan Plateau since Mesozoic with implications for the plateau growth. Journal of Asian Earth Sciences, 198, 104131.

O'Sullivan, P.B., Parrish, R.R., 1995. The importance of apatite composition and single grain ages when interpreting fission track data from plutonic rocks: a case study from the Coast Ranges, British Columbia. Earth and Planetary Science Letters

132 (1), 213-224.

Pan, B., Li, Q., Hu, X., Gao, H., Li, Z. 2013. Cretaceous and Cenozoic cooling history of the eastern Qilian Shan, north-eastern margin of the Tibetan Plateau: evidence from apatite fission-track analysis. Terra Nova, 25, 431-438.

Pang, J., Yu, J., Zheng, D., Wang, W., Ma, Y., Wang, Y., Li, C., Li, Y., Wang, Y. 2019. Neogene Expansion of the Qilian Shan, North Tibet: Implications for the Dynamic Evolution of the Tibetan Plateau. Tectonics, 38, 1018-1052.

Peng, H., Wang, J., Liu, C., Zhang, S., Zattin, M., Wu, N., Feng, Q. 2019. Thermochronological constraints on the Meso-Cenozoic tectonic evolution of the Haiyuan-Liupanshan region, northeastern Tibetan Plateau. Journal of Asian Earth Sciences, 183, 103966.

Perrineau, A., Van Der Woerd, J., Gaudemer, Y., Liu-Zeng, J., Pik, R., Tapponnier, P., Rong, Z. 2011. Incision rate of the Yellow River in Northeastern Tibet constrained by ^{10}Be and ^{26}Al cosmogenic isotope dating of fluvial terraces: implications for catchment evolution and plateau building. Geological Society, London, Special Publications, 353(1), 189-219.

Qinghai Geologic Bureau, 1989. Regional Geology Evolution of Gansu Province. Geological Publishing House, Beijing, pp. 1-526 (in Chinese with English abstract).

Qi, B., Hu, D., Yang, X., Zhang, Y., Tan, C., Zhang, P., Feng, C., 2016. Apatite fission track evidence for the Cretaceous-Cenozoic cooling history of the Qilian Shan (NW China) and for stepwise northeastward growth of the northeastern Tibetan

Plateau since early Eocene. Journal of Asian Earth Science. 124, 28-41.

Vincent, S. J., Allen, M. B. 1999. Evolution of the Minle and Chaoshui Basins, China: Implications for Mesozoic strike-slip basin formation in Central Asia. Geological Society of America Bulletin, 111, 725-742.

Vermeesch, P., 2009. RadialPlotter: a Java application for fission track, luminescence and other radial plots. Radiat. Meas. 44, 409-410.

Wang, F., Lo, C. H., Li, Q., Yeh, M. W., Wan, J., Zheng, D. 2004. Onset timing of significant unroofing around Qaidam basin, northern Tibet, China: constraints from 40Ar/39Ar and FT thermochronology on granitoids. Journal of Asian Earth Sciences, 24(1), 59-69.

Wang, C., Zhao, X., Liu, Z., Lippert, P. C., Graham, S. A., Coe, R. S., Li, Y. 2008. Constraints on the early uplift history of the Tibetan Plateau. Proceedings of the National Academy of Sciences, 105(13), 4987-4992.

Wang, X., Lu, H., Vandenberghe, J., Zheng, S., Balen, R. V. 2012. Late Miocene uplift of the Tibetan Plateau inferred from basin filling, planation and fluvial terraces in the Huang Shui catchment. Global Planetary Change, 88, 10-19.

Wang, X., Song, C., Zattin, M., He, P., Song, A., Li, J., Wang, Q. 2016a. Cenozoic pulsed deformation history of northeastern Tibetan Plateau reconstructed from fission-track thermochronology. Tectonophysics, 88, 367-370.

Wang, W., Zhang, P., Pang, J., Garzione, C., Zhang, H., Liu, C. 2016b. The Cenozoic growth of the Qilian Shan in the northeastern Tibetan Plateau: a sedimentary archive from the Jiuxi Basin. Journal of Geophysical Research Solid Earth, 121, 2235-2257.

Wang, X., Deng, L., Zattin, M., Ji, M., Li, J. 2017a. Palaeogene growth of the northeastern Tibetan Plateau: Detrital fission track and sedimentary analysis of the Lanzhou Basin, NW China. Journal of Asian Earth Sciences, 147, 322-331.

Wang, W., Qiao, X., Yang, S., Wang, D. 2017b. Present-day velocity field and block kinematics of Tibetan Plateau from GPS measurements. Geophysical Journal International, 208, 1088-1102.

Wang, F., Shi, W., Zhang, W., Wu, L., Yang, L., Wang, Y., Zhu, R. 2017c. Differential growth of the northern Tibetan margin: evidence for oblique stepwise rise of the Tibetan Plateau. Scientific reports, 7(1), 1-9.

Wang, Y., Zheng, J., Zheng, Y. 2018. Mesozoic-Cenozoic exhumation history of the Qimen Tagh Range, northeastern margins of the Tibetan Plateau: Evidence from apatite fission track analysis. Gondwana Research, 58, 16-26.

Wang, W., Zheng, D., Li, C., Wang, Y., Zhang, Z., Pang, J., Zhang, H. 2020. Cenozoic exhumation of the Qilian Shan in the northeastern Tibetan Plateau: Evidence from low-temperature thermochronology. Tectonics, 39(4), e2019TC005705.

Wu, L., Xiao, A., Yang, S., Wang, L., Mao, L., Wang, L., Xu, B. 2012. Two-stage evolution of the Altyn Tagh Fault during the Cenozoic: new insight from provenance analysis of a geological section in NW Qaidam Basin, NW China. Terra Nova, 24(5), 387-395.

Xiao, W., Windley, B. F., Yong, Y., Yan, Z., Yuan, C., Liu, C. 2009. Early Paleozoic to Devonian multiple-accretionary model for the Qilian Shan, NW China. Journal of Asian Earth Sciences, 35, 323-333.

Xiao, G., Guo, Z., Dupont-Nivet, G., Lu, H., Wu, N., Ge, J. 2012. Evidence for Northeastern Tibetan Plateau uplift between 25 and 20 Ma in the sedimentary archive of the Xining Basin, northwestern China. Earth Planetary Science Letters, 317, 185-195.

Xu, Zh., Yang, J., Wu, C., Li, H., Zhang, J., Qi, X., Song, Sh., Qiu, H. 2006. Timing and mechanism of formation and exhumation of the Northern Qaidam ultrahigh-pressure metamorphic belt. Journal of Asian Earth Sciences, 28, 160-173.

Yang, J., Xu, Z., Zhang, J., Chu, C. Y., Zhang, R., Liou, J. G. 2001. Tectonic significance of early Paleozoic high-pressure rocks in Altun-Qaidam-Qilian Mountains, northwest China. Memoirs-Geological Society of America, 151-170.

Yin, A., Harrison, T.M. 2000. Geologic evolution of the Himalayan-Tibetan orogen. Annual Review of Earth and Planetary Sciences, 28, 211-280.

Yin, A., Rumelhart, P.E., Butler, R., Cowgill, E., Harrison, T.M., Foster, D.A., Ingersoll, R.V., Qing, Z., Xian, Z., Xiao, W., Hanson, A., Raza, A., 2002. Tectonic history of the Altyn Tagh fault system in northern Tibet inferred from Cenozoic sedimentation. Geological Society of America Bulletin, 114, 1257-1295.

Yin, A., Dang, Y. Q., Wang, L. C., Jiang, W. M., Zhou, S. P., Chen, X. H., McRivette, M. W. 2008a. Cenozoic tectonic evolution of Qaidam basin and its surrounding regions (Part 1): The southern Qilian Shan-Nan Shan thrust belt and northern Qaidam basin. Geological Society of America Bulletin, 120(7-8), 813-846.

Yin, A., Dang, Y. Q., Zhang, M., Chen, X. H., McRivette, M. W. 2008b. Cenozoic tectonic evolution of the Qaidam basin and its surrounding regions (Part 3):

Structural geology, sedimentation, and regional tectonic reconstruction. Geological Society of America Bulletin, 120(7-8), 847-876.

Yuan, W., Dong, J., Wang, S., Carter, A. 2006. Apatite fission track evidence for Neogene uplift in the eastern Kunlun mountains, northern Qinghai-Tibet Plateau, China. Journal of Asian Earth Sciences, 27, 847-856.

Yu, J., Pang, J., Wang, Y., Zheng, D., Liu, C., Wang, W. 2019a. Mid-Miocene uplift of the northern Qilian Shan as a result of the northward growth of the northern Tibetan Plateau. Geosphere, 15, 423-432.

Yu, J., Zheng, D., Pang, J., Wang, Y., Fox, M., Vermeesch, P., Wang, Y. 2019b. Miocene Range Growth Along the Altyn Tagh Fault: Insights From Apatite Fission Track and (U-Th)/He Thermochronometry in the Western Danghenan Shan, China. Journal of Geophysical Research: Solid Earth, 124(8), 9433-9453.

Zattin, M., Wang, X. 2019. Exhumation of the western Qinling mountain range and the building of the northeastern margin of the Tibetan Plateau. Journal of Asian Earth Sciences, 177, 307-313.

Zeng, L., Zhang, K. J., Tang, X. C., Zhang, Y. X., Li, Z. W. 2018. Mid-Permian rifting in Central China: Record of geochronology, geochemistry and Sr-Nd-Hf isotopes of bimodal magmatism on NE Qinghai-Tibetan Plateau. Gondwana Research, 57, 77-89.

Zhang, B., Zhang, J., Wang, Y., Zhao, H., Li, Y. 2017. Late Mesozoic-Cenozoic Exhumation of the Northern Hexi Corridor: Constrained by Apatite Fission Track Ages of the Longshoushan. Acta Geologica Sinica-English Edition, 91(5),

1624-1643.

Zhang, H. P., Craddock, W. H., Lease, R. O., Wang, W. T., Yuan, D. Y., Zhang, P. Z. 2012. Magnetostratigraphy of the Neogene Chaka basin and its implications for mountain building processes in the north-eastern Tibetan Plateau. Basin Research, 24, 31-50.

Zhang, H., Zhang, P., Champagnac, J. D., Molnar, P., Anderson, R. S., Kirby, E., Liu, S. 2014. Pleistocene drainage reorganization driven by the isostatic response to deep incision into the northeastern Tibetan Plateau. Geology, 42(4), 303-306.

Zhang, H. P., Oskin, M. E., Liu-Zeng, J., Zhang, P., Reiners, P. W., Xiao, P. 2016. Pulsed exhumation of interior eastern Tibet: implications for relief generation mechanisms and the origin of high-elevation planation surfaces. Earth and Planetary Science Letters, 449, 176-185.

Zhang, H., Yang, T., Hou, Z., Wang, Y. 2020a. Magmatic expression of tectonic transition from oceanic subduction to continental collision: Insights from the Middle Triassic rhyolites of the North Qiangtang Block. Gondwana Research, in press.

Zhang, C., Wu, L., Chen, W., Zhang, Y., Xiao, A., Zhang, J., Chen, H. 2020b. Early Cretaceous foreland-like Northeastern Qaidam Basin, Tibetan Plateau and its tectonic implications: Insights from sedimentary investigations, detrital zircon U-Pb analyses and seismic profiling. Palaeogeography, Palaeoclimatology, Palaeoecology, 109912.

Zhang, X., Chung, S. L., Lai, Y. M., Ghani, A. A., Murtadha, S., Lee, H. Y., Hsu, C. C. 2019. A 6000-km-long Neo-Tethyan arc system with coherent magmatic flare-ups and lulls in South Asia. Geology, 47(6), 573-576.

Zhuang, G., Johnstone, S. A., Hourigan, J., Ritts, B., Robinson, A., Sobel, E. R. 2018. Understanding the geologic evolution of Northern Tibetan Plateau with multiple thermochronometers. Gondwana Research, 58, 195-210.

Zheng, D., Clark, M.K., Zhang, P., Zheng, W., Farley, K.A., 2010. Erosion, fault initiation and topographic growth of the North Qilian Shan (northern Tibetan Plateau). Geosphere, 6, 937-941.

Zheng, D., Wang, W., Wan, J., Yuan, D., Liu, C., Zheng, W., Zhang, P. 2017. Progressive northward growth of the northern Qilian Shan-Hexi Corridor (northeastern Tibet) during the Cenozoic. Lithosphere, 9, 408-416.

Zheng, H., Clift, P. D., Wang, P., Tada, R., Jia, J., He, M., Jourdan, F. 2013. Pre-miocene birth of the Yangtze River. Proceedings of the National Academy of Sciences, 110(19), 7556-7561.

Zuza, A. V., Cheng, X., Yin, A. 2016. Testing models of Tibetan Plateau formation with Cenozoic shortening estimates across the Qilian Shan-Nan Shan thrust belt. Geosphere, 12, 501-532.

Zuza, A. V., Wu, C., Reith, R. C., Yin, A., Liu, W. 2018. Tectonic evolution of the Qilian Shan: an early Paleozoic orogen reactivated in the Cenozoic. Geological Society of America Bulletin, 130, 881-925.

Zuza, A. V., Wu, C., Wang, Z., Levy, D. A., Li, B., Xiong, X., Chen, X. 2019. Underthrusting and duplexing beneath the northern Tibetan Plateau and the evolution of the Himalayan-Tibetan orogen. Lithosphere, 11(2), 209-231.

Figure captions

Fig. 1 (a) Sketch map of the major blocks and suture zones of Tibetan Plateau and adjacent regions (after Yin and Harrison, 2000; Tapponnier et al., 2001). The red arrows indicate where the plate is moving (after Wang et al., 2017b). (b) Topography and major faults in the northeastern Tibetan Plateau. NQS=North Qilian Shan, TLS=Tuole Shan, TLNS=Tuole Nan Shan, SLNS=Shule Nan Shan, CQS=Central Qilian Shan, LJS=Laji Shan, DHNS= Danghe Nan Shan, ZWLS=Zongwulong Shan, QHNS=Qinghai Nan Shan, GHNS=Gonghe Nan Shan, WQL=West Qinglin. (c) Topographic profile along the transect A-A'. Yellow dots denote the locations of samples from the Eastern Qinghai Nan Shan. See Fig. 1b for location of A-A'.

Fig. 2 Simplified geologic map of the Qinghai Nan Shan and adjacent areas (modified from the 1:2.5 million scale geologic map of China (China Geological Survey, 2004)).

Fig. 3 Detailed geologic map of the study area, with sample locations shown as white squares. The late Cenozoic strata, overlying the Mesozoic granitoids (Zeng et al., 2018), are distributed on the north and south sides of Longyang Gorge unconformably.

Fig. 4 Radial plots constructed using RadialPlotter software (Vermeesch, 2009) for AFT ages from the Eastern Qinghai Nan Shan.

Fig. 5 AFT and AHe cooling ages vs. elevations for eastern (our data) and central (Craddock, 2011) part of the Qinghai Nan Shan. Dashed lines outline age-elevation trend.

Fig. 6 Plots of (A) AFT age and (B) track length vs. D_{par}. Dpar is the arithmetic mean fission-track etch figure diameter parallel to the crystallographic c-axis (Donelick et al., 2005).

Fig. 7 Plots of AHe ages vs. eU (eU=effective U concentration) (A) and Rs (sphere equivalent radius) (B).

Fig. 8 AFT thermal history models obtained for the Eastern Qinghai Nan Shan vertical transect samples produced using HeFTy (Ketcham, 2005).The pink and green envelope represents a good fit and an acceptable fit. The black line corresponds to the "best fit model" line. Black rectangles are the constraint boxes. T-t constraints imposed into the modeling were described in the text. PAZ: partial annealing zone of apatite fission track.

Fig. 9 AHe thermal history modeling using HeFTy software (Ketcham, 2005) for the Eastern Qinghai Nan Shan vertical transect samples. Results presented as envelopes surrounding good (pink) and acceptable (green) fitting histories, and black lines are corresponds to the "best fit model" line. Black boxes indicate time-temperature constraints. The detailed T-t constraints were described in the text. PRZ: partial retention zone of helium.

Fig. 10 Shown are distribution of major AFT or AHe and sedimentary studying locations and results.

Table1. Information of the samples reported in this study

Sample	Lithology	Altitude (m)	Latitude	Longitude
HR-6	Indosinian granite	3270	36°17′25″	100°51′16″
HR-7	Indosinian granite	3061	36°14′45″	100°51′58″
HR-8	Indosinian granite	2734	36°08′40″	100°55′04″
HR-9	Indosinian granite	2537	36°08′29″	101°02′19″
LY-1	Indosinian granite	2450	36°07′51"	100°59'45"
LY-2	Indosinian granite	2409	36°07'48"	100°59'56"
LY-3	Indosinian granite	2350	36°07'30"	100°59'30"

Table 2 Measured apatite fission track data in this study

Sample	**N(grains)**	**n(tracks)**	**ρ_s (Ns)**	**ρ_{STD}**	**Zeta**	**U-UNK**	**U-STD**	**P(χ^2)**	**Dpar**	**Age**	**L±SD(n)**
			×10E+6	**×10E+5**	**×10E-3**	**ug/g**	**μg/g**		**μm**	**Ma (±1σ)**	**μm**
HR-6	37	457	0.56	1.63	1.79	8.5	9.22	0.35	2.99	180±11	11.93±2.55(63)
HR-7	31	521	1.05	1.63	2.31	14.9	10.99	0.86	1.61	165.6±9.5	13.18±1.85(48)
HR-9	24	373	0.99	1.63	1.75	15.5	9.04	0.00	2.63	169±18	12.12±2.17(64)
LY-1	39	719	1.16	1.98	1.59	19.68	9.98	0.11	1.94	114.3±7.9	13.23±1.53(57)
LY-2	38	607	1.02	1.98	1.59	13.49	9.98	0.46	2.42	122.7±6.6	12.64±1.98(56)
LY-3	31	453	0.95	1.98	1.64	16.48	10.27	0.10	1.92	119.1±7.8	13.07±1.55(54)

N(grains): number of apatite crystals analyzed; n(tracks): number of apatite fission track analyzed; $\rho_{s\,(Ns)}$ and ρ_{STD}: spontaneous fission-track density of apatite crystals analyzed of samples and standards; Zeta: LA-ICP-MS calibration factor determined against Dur-2 standards; U-UNK and U-STD: uranium-238 concentration of samples and Dur-2 standards measured by LA-ICP-MS; P(χ^2): chi-squared probability; Dpar: mean diameter of fission-track etch images parallel to the crystallographic c-axis. L±SD: mean track length+ standard deviation, n, number of tracks measured.

Table 3 Results of single grain AHe dating in this study

Sample	**length**	**width**	**Mass**	**Rs**	**^{4}He**	**U**	**Th**	**Sm**	**eU**	**Th/ U**	**Raw age**	**Ft**	**Corr. age**	**Error (±1σ)**	**Mean age (±1σ)**
	μm	**μm**	**mg**	**μm**	**nmol/g**	**ppm**	**ppm**	**ppm**	**ppm**		**Ma**		**Ma**	**Ma**	**Ma**
HR-6															
G-1	298	111.3	6.55	64.45	8.232	12.54	31.11	30.44	19.8	2.48	75.3	0.77	97.5	1.3	
G-2	274.8	134.9	7.37	71.35	19.402	30.06	70.31	36.22	46.6	2.33	76.1	0.79	95.9	1.3	97.7±1.6

G-3	225.2	107.6	3.07	50.26	12.184	20.27	46.17	45.19	31.1	2.27	71.2	0.71	99.9	1.7	
HR-7															
G-1	162.2	77.4	1.26	38.19	29.528	48.29	113.99	57.3	75.1	2.36	71.9	0.68	115.4	1.6	
G-2	165.6	108.4	1.83	45.46	17.841	28.44	63.89	60.13	43.5	2.24	74.7	0.68	108.9	2.2	
G-3	151.9	62.9	1.02	35.33	10.801	19.33	61.91	37.98	33.9	3.20	58.1	0.58	98.7	3.3	107.6±2.4
HR-8															
G-1	231.2	144.7	6.75	72.82	9.118	15.42	21.43	27.59	20.5	1.39	81.1	0.80	100.8	1.7	
G-2	243.9	116.4	5.67	66.43	23.957	30.43	49.75	44.58	42.1	1.63	103.5	0.78	132.1	1.3	
G-3	214.1	154	5.96	70.43	21.375	37.69	45.28	38.98	48.3	1.20	80.8	0.79	101.2	1.1	111.3±1.5
HR-9															
G-1	214.3	90.6	3.05	51.57	12.496	35.55	102.56	48.51	59.7	2.88	38.3	0.71	53.6	0.8	
G-2	155.4	83.4	1.59	43.51	9.129	38.05	123.42	65.22	67	3.[illegible]4	24.9	0.66	37.5	0.5	
G-3	225.4	45.6	1.29	33.71	7.151	38.24	106.14	64.35	63.2	2.77	20.7	0.56	36.6	0.5	42.5±0.6
LY-1															
G-1	175.4	90.8	2.86	49.9	11.428	28.93	15.6	43.95	32.6	[illegible]53	87.2	0.72	137.8	3.8	
G-2	133.8	83.5	1.98	42.7	16.513	37.13	14.33	50.59	40.[illegible]	[illegible].38	101.1	0.67	159.1	7.3	
G-3	196	110.2	5.52	64.06	19.063	23.85	12.37	36.28	2[illegible].[illegible]	0.51	55.1	0.78	87.1	5.9	128.0±5.9
LY-2															
G-1	162.1	87	2.44	48.61	16.414	31.04	45.8	64.04	41.8	1.47	71.4	0.70	114.3	4.3	
G-2	120.8	102.2	2.77	49.55	15.758	26.16	17.09	46.[illegible]	30.2	0.65	94.8	0.72	149.9	4.3	
G-3	132.3	79.4	2.37	46.18	0.146	0	0	[illegible].03	0	N/A	N/A	0.69	N/A	N/A	
G-4	131	95.4	2.26	48.29	14.119	30.05	2[illegible]68	58.34	36.3	0.88	70.7	0.71	112.2	5.5	
G-5	13.4	102.2	1.73	42.23	21.089	55.78	24.11	84.45	61.4	0.43	62.6	0.68	98.8	6.4	118.8±4.9
LY-3															
G-1	155.2	51.4	1.15	35.28	14.209	22.6[illegible]	[illegible].09	75	32.1	1.77	80.0	0.59	128.1	9.2	
G-2	122.3	79.4	2.19	45.12	28.468	[illegible].58	41.53	55.03	78.3	0.60	66.6	0.69	105.6	4.4	
G-3	135.9	63.8	1.31	38.55	23.937	51.[illegible]	51.6	78.13	64.1	0.99	68.1	0.63	108.5	6.5	
G-4	123.3	101.7	3.11	51.33	16.229	[illegible].83	23.51	39.3	51.4	0.51	57.9	0.73	91.7	1.6	
G-5	135.3	81.4	1.19	37.44	30.76[illegible]	[illegible].19	59.45	84.96	79.2	0.91	71	0.63	112.9	3.1	109.3±2.6

Conflict of interest statement

The authors declare that they have no known competing financial interests or personal relationships that could have appeared to influence the work reported in this paper.

Highlights

• Low-temperature thermochronological study was carried out for Yellow River valley.

• Eastern Qinghai Nan Shan experienced rapid exhumation since the late Mesozoic.

• Geomorphic framework of the NE Tibetan Plateau was initially established since the late Mesozoic.

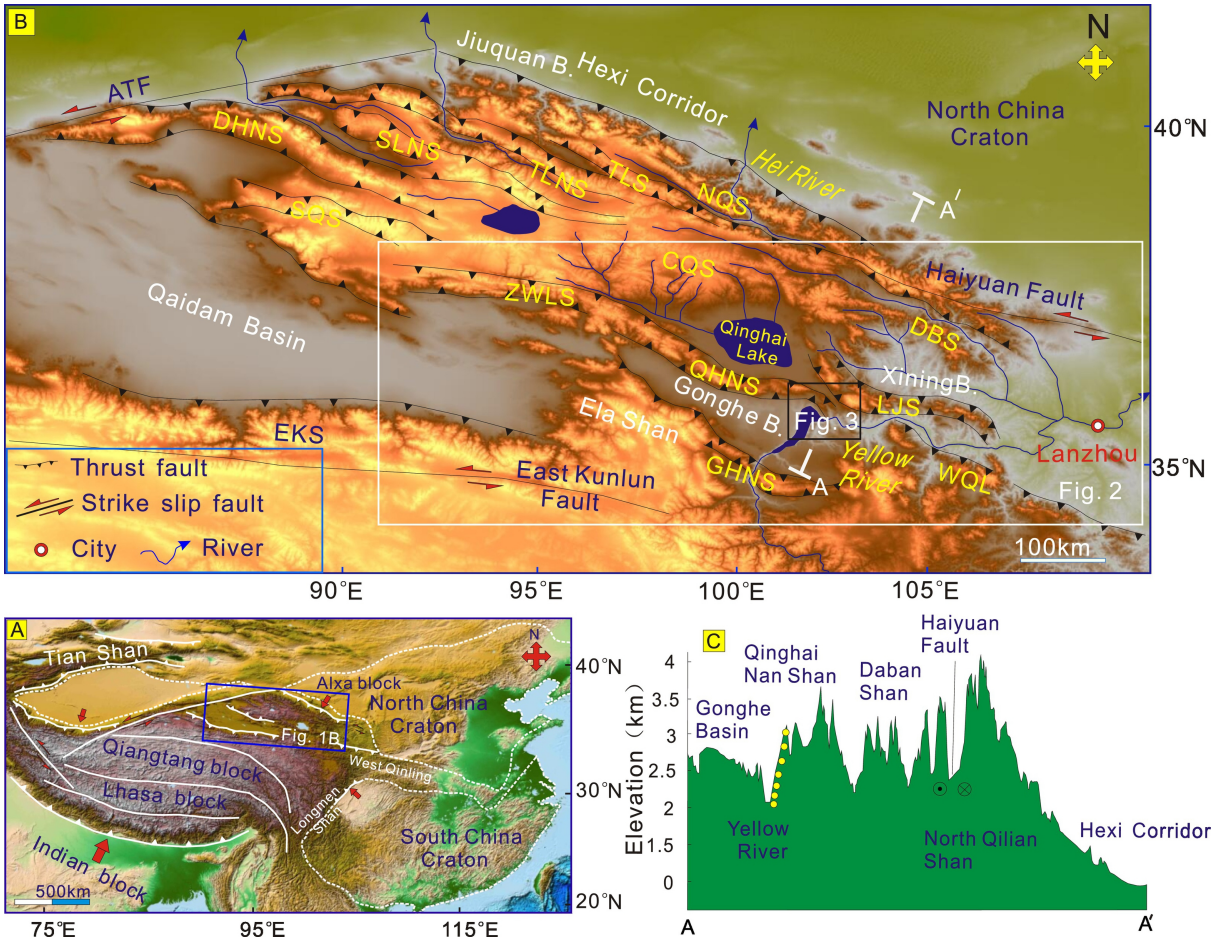
B
N
ATF
Jiuquan B.
Hexi Corridor
North China Craton
Hei River
A′
DHNS
SLNS
TLNS
TLS
NQS
QQS
CQS
zWLS
Haiyuan Fault
Qaidam Basin
Qinghai Lake
DBS
QHNS
XiningB.
Gonghe B.
Fig. 3
LJS
Ela Shan
EKS
Yellow River
Lanzhou
GHNS
A
WQL
Fig. 2
East Kunlun Fault
Thrust fault
Strike slip fault
City
River
100km
40°N
35°N
90°E
95°E
100°E
105°E
A
Tian Shan
N
Alxa block
North China Craton
Fig. 1B
Qiangtang block
West Qinling
Lhasa block
Longmen Shan
South China Craton
Indian block
500km
40°N
30°N
20°N
75°E
95°E
115°E
C
Haiyuan Fault
Qinghai Nan Shan
Daban Shan
Gonghe Basin
Elevation (km)
4
3.5
3
2.5
2
1.5
0
Yellow River
North Qilian Shan
Hexi Corridor
A
A′

Figure 1

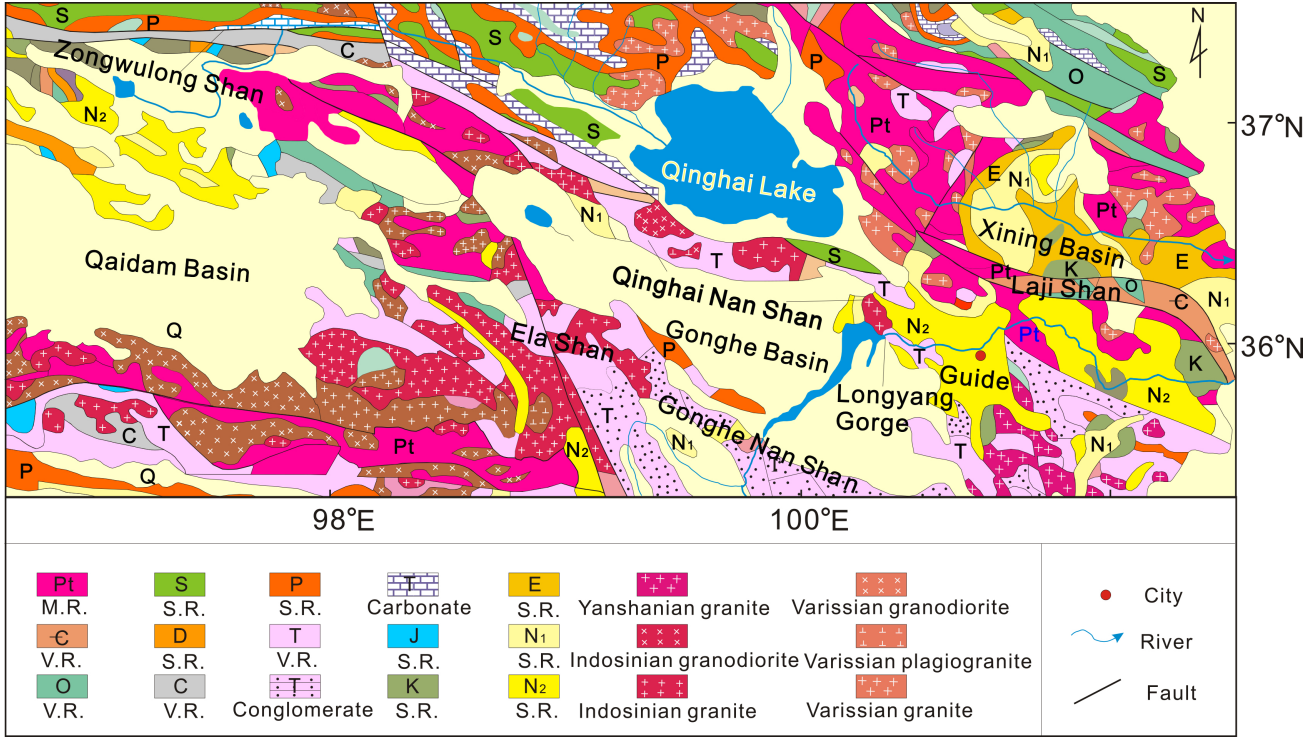
Zongwulong Shan
Qaidam Basin
Qinghai Lake
Qinghai Nan Shan
Ela Shan
Gonghe Basin
Gonghe Nan Shan
Longyang Gorge
Guide
Xining Basin
Laji Shan
N
37°N
36°N
98°E
100°E
M.R.
S.R.
V.R.
Carbonate
Conglomerate
Yanshanian granite
Indosinian granodiorite
Indosinian granite
Varissian granodiorite
Varissian plagiogranite
Varissian granite
City
River
Fault

Figure 2

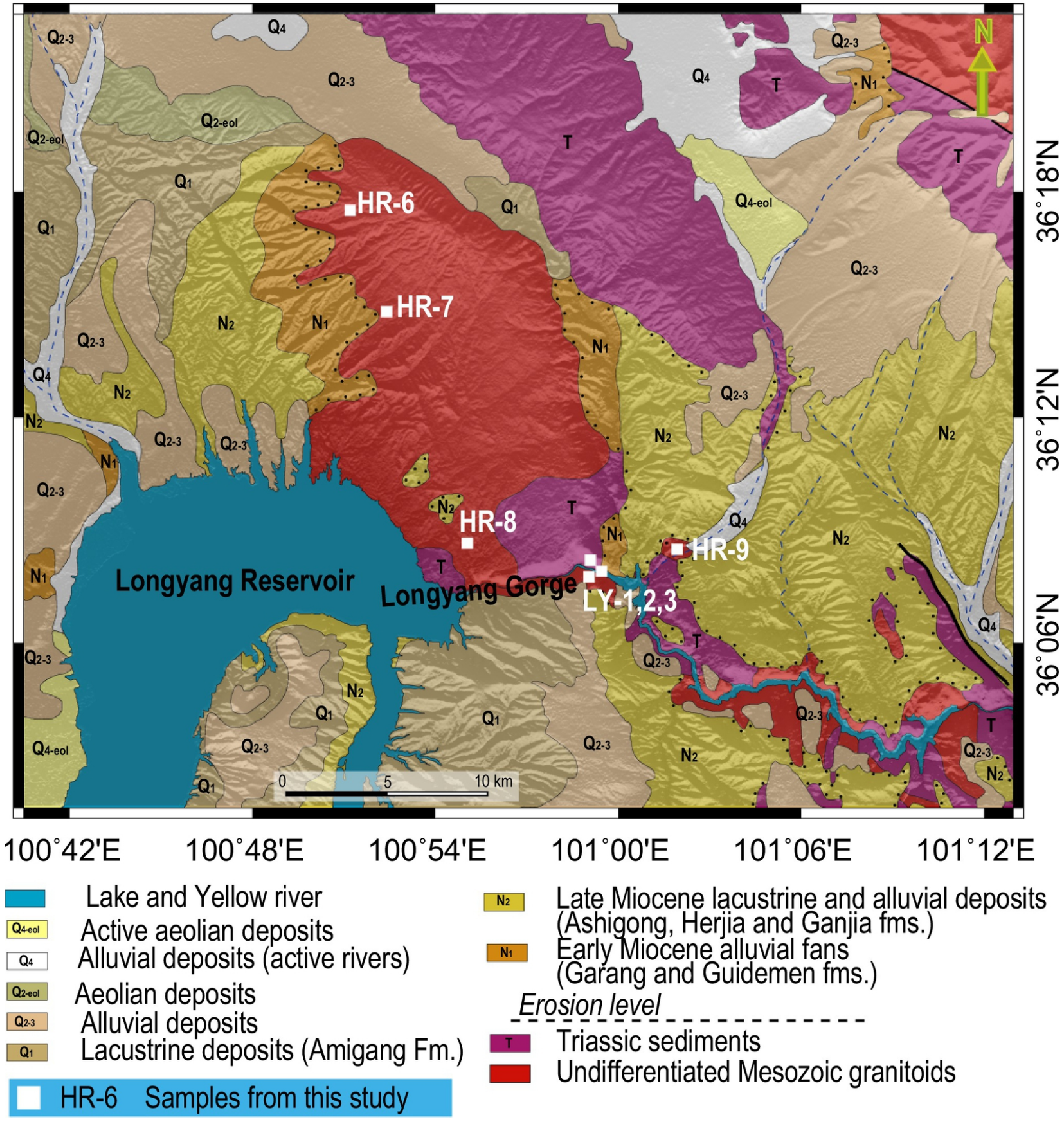
HR-6
HR-7
HR-8
HR-9
LY-1,2,3
Longyang Reservoir
Longyang Gorge
N
0
5
10 km
36°18'N
36°12'N
36°06'N
100°42'E
100°48'E
100°54'E
101°00'E
101°06'E
101°12'E
Lake and Yellow river
Active aeolian deposits
Alluvial deposits (active rivers)
Aeolian deposits
Alluvial deposits
Lacustrine deposits (Amigang Fm.)
HR-6 Samples from this study
Late Miocene lacustrine and alluvial deposits (Ashigong, Herjia and Ganjia fms.)
Early Miocene alluvial fans (Garang and Guidemen fms.)
Erosion level
Triassic sediments
Undifferentiated Mesozoic granitoids

Figure 3

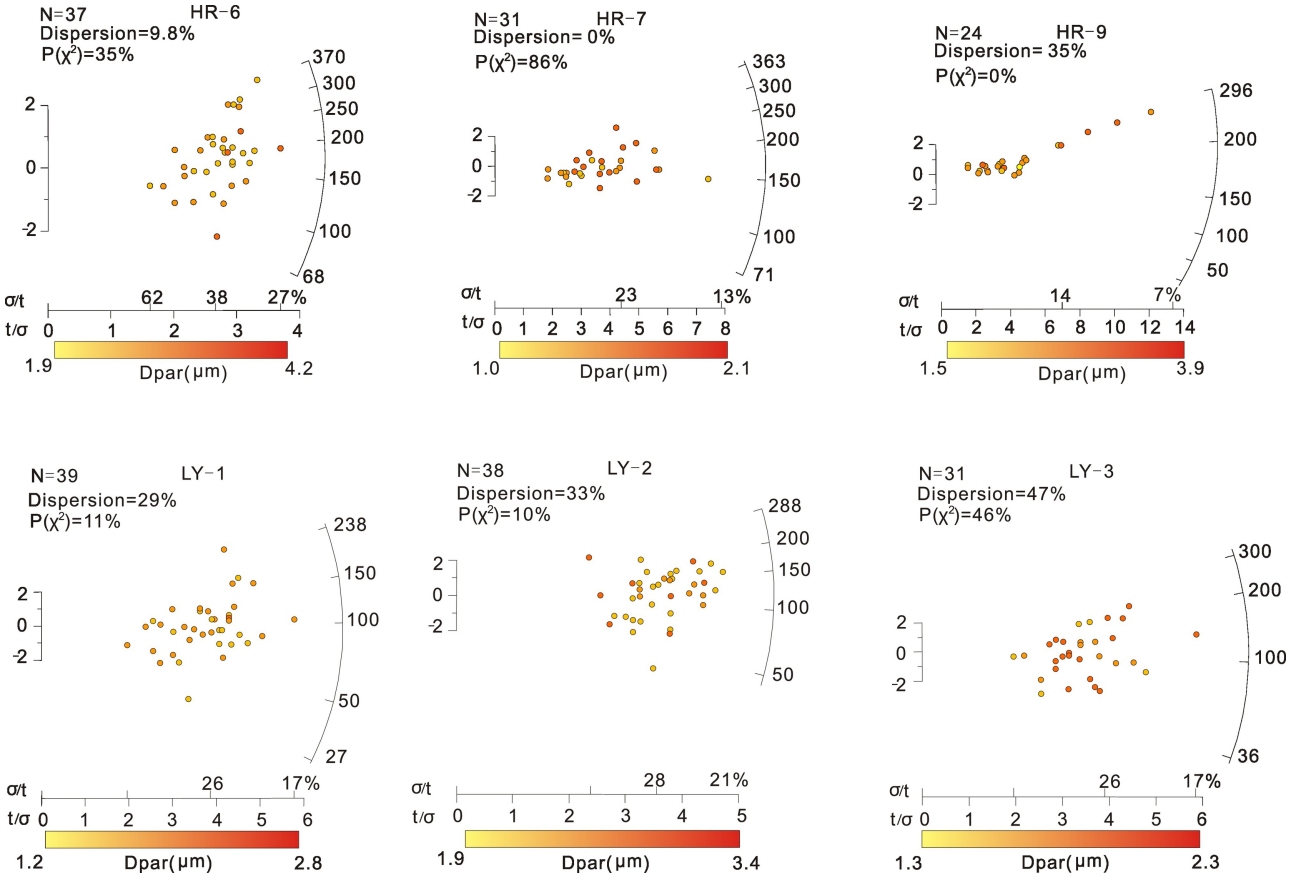
N=37 HR-6
Dispersion=9.8%
P(χ²)=35%
370 300 250 200 150 100 68
2 0 -2
σ/t 62 38 27%
t/σ 0 1 2 3 4
1.9 Dpar(μm) 4.2
N=31 HR-7
Dispersion= 0%
P(χ²)=86%
363 300 250 200 150 100 71
2 0 -2
σ/t 23 13%
t/σ 0 1 2 3 4 5 6 7 8
1.0 Dpar(μm) 2.1
N=24 HR-9
Dispersion= 35%
P(χ²)=0%
296 200 150 100 50
2 0 -2
σ/t 14 7%
t/σ 0 2 4 6 8 10 12 14
1.5 Dpar(μm) 3.9
N=39 LY-1
Dispersion=29%
P(χ²)=11%
238 150 100 50 27
2 0 -2
σ/t 26 17%
t/σ 0 1 2 3 4 5 6
1.2 Dpar(μm) 2.8
N=38 LY-2
Dispersion=33%
P(χ²)=10%
288 200 150 100 50
2 0 -2
σ/t 28 21%
t/σ 0 1 2 3 4 5
1.9 Dpar(μm) 3.4
N=31 LY-3
Dispersion=47%
P(χ²)=46%
300 200 100 36
2 0 -2
σ/t 26 17%
t/σ 0 1 2 3 4 5 6
1.3 Dpar(μm) 2.3

Figure 4

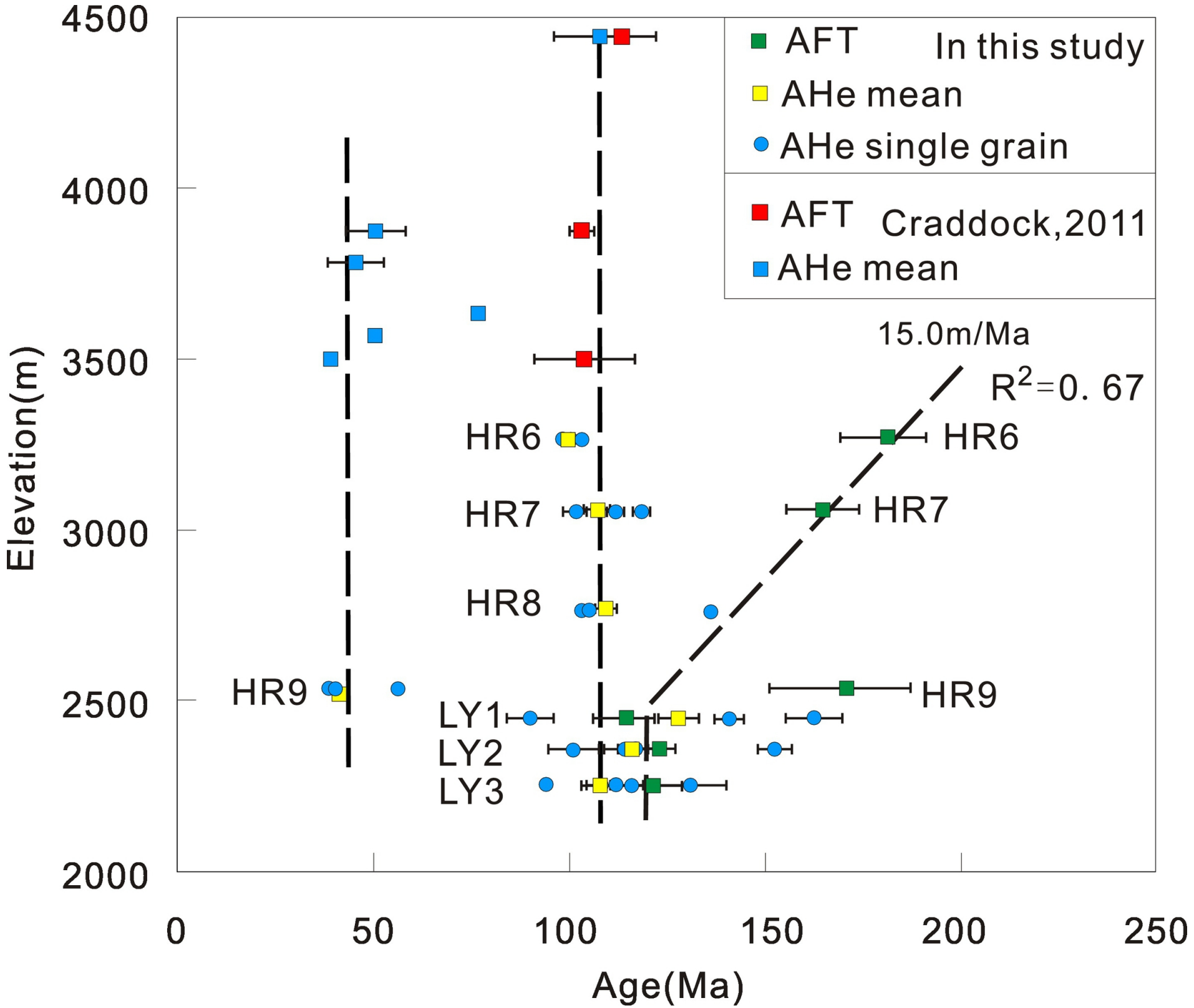
4500
4000
3500
3000
2500
2000
Elevation(m)
0
50
100
150
200
250
Age(Ma)
AFT
In this study
AHe mean
AHe single grain
AFT
Craddock,2011
AHe mean
15.0m/Ma
R2=0. 67
HR6
HR7
HR8
HR9
LY1
LY2
LY3
HR6
HR7
HR9

Figure 5

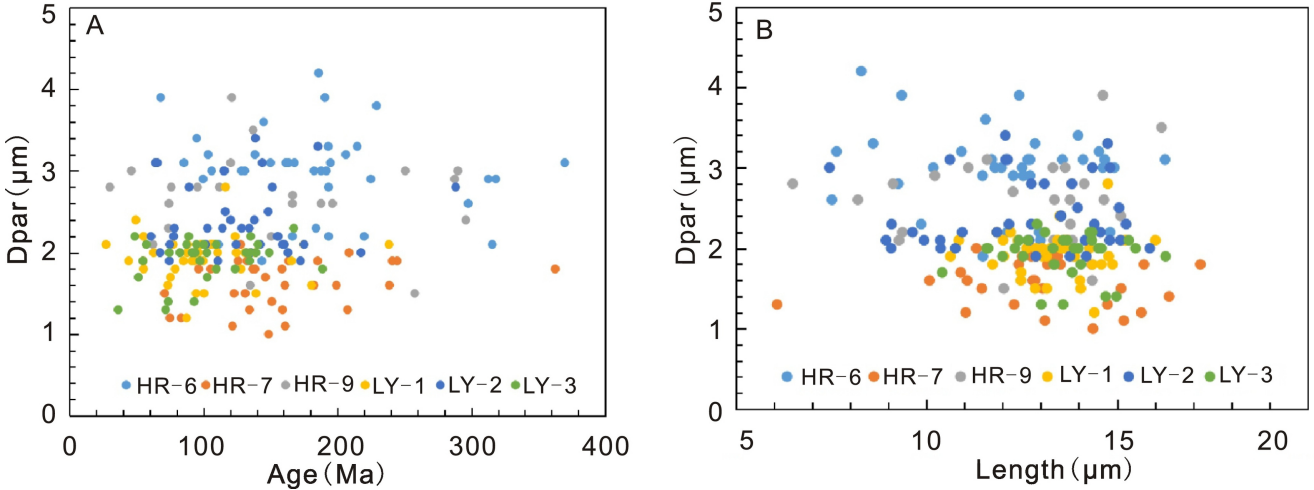
A
Dpar (μm)
Age (Ma)
HR-6
HR-7
HR-9
LY-1
LY-2
LY-3
B
Dpar (μm)
Length (μm)
HR-6
HR-7
HR-9
LY-1
LY-2
LY-3

Figure 6

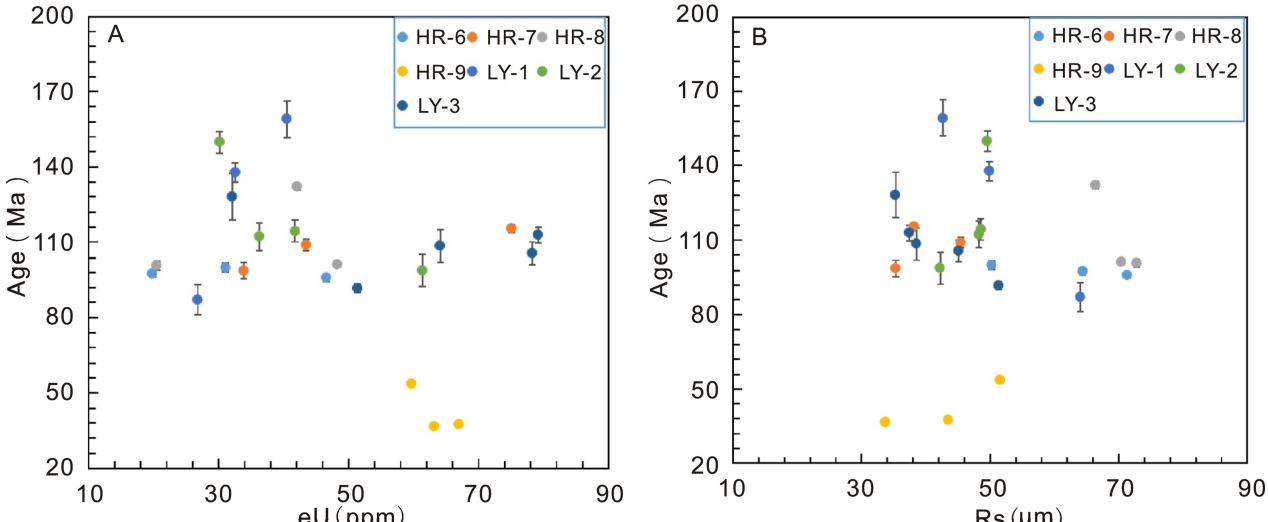
A
B
HR-6
HR-7
HR-8
HR-9
LY-1
LY-2
LY-3
Age (Ma)
eU (ppm)
Rs (μm)
200
170
140
110
80
50
20
10
30
50
70
90

Figure 7

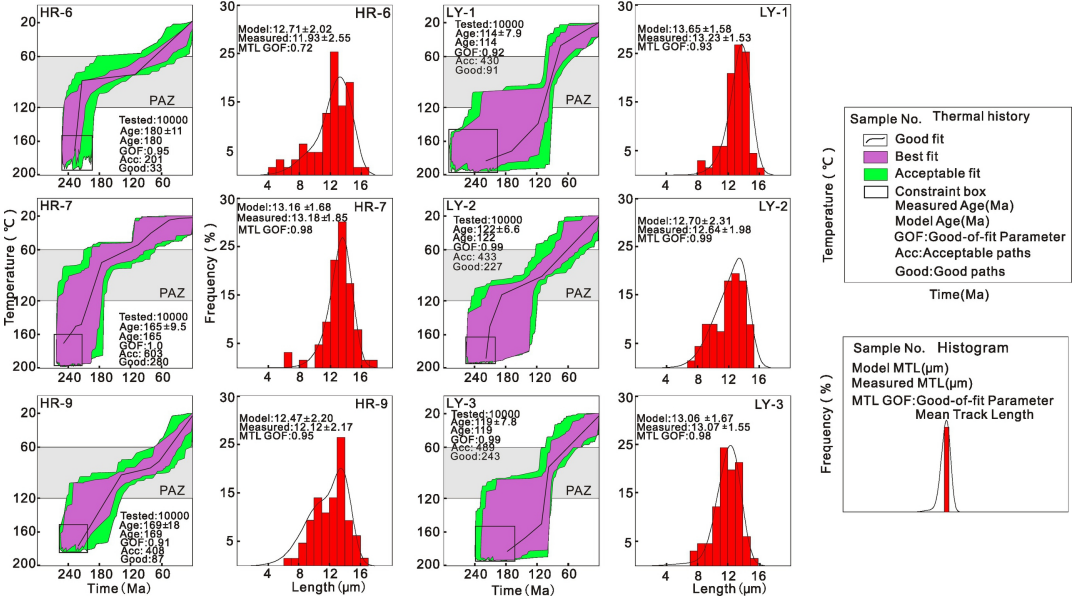
HR-6
PAZ
Tested:10000
Age:180±11
Age:180
GOF:0.95
Acc: 201
Good:33
HR-6
Model:12.71±2.02
Measured:11.93±2.55
MTL GOF:0.72
LY-1
Tested:10000
Age:114±7.9
Age:114
GOF:0.92
Acc: 430
Good:91
LY-1
Model:13.65±1.58
Measured:13.23±1.53
MTL GOF:0.93
HR-7
PAZ
Tested:10000
Age:165±9.5
Age:165
GOF:1.0
Acc: 893
Good:280
HR-7
Model:13.16 ±1.68
Measured:13.18±1.85
MTL GOF:0.98
LY-2
Tested:10000
Age:122±6.6
Age:122
GOF:0.99
Acc: 433
Good:227
LY-2
Model:12.70±2.31
Measured:12.64±1.98
MTL GOF:0.99
HR-9
PAZ
Tested:10000
Age:169±18
Age:169
GOF:0.91
Acc: 408
Good:87
HR-9
Model:12.47±2.20
Measured:12.12±2.17
MTL GOF:0.95
LY-3
Tested:10000
Age:119±7.8
Age:119
GOF:0.99
Acc: 488
Good:243
LY-3
Model:13.06 ±1.67
Measured:13.07 ±1.55
MTL GOF:0.98
Temperature (℃)
Frequency (%)
Time (Ma)
Length (μm)
Sample No. Thermal history
Good fit
Best fit
Acceptable fit
Constraint box
Measured Age(Ma)
Model Age(Ma)
GOF:Good-of-fit Parameter
Acc:Acceptable paths
Good:Good paths
Time(Ma)
Sample No. Histogram
Model MTL(μm)
Measured MTL(μm)
MTL GOF:Good-of-fit Parameter
Mean Track Length

Figure 8

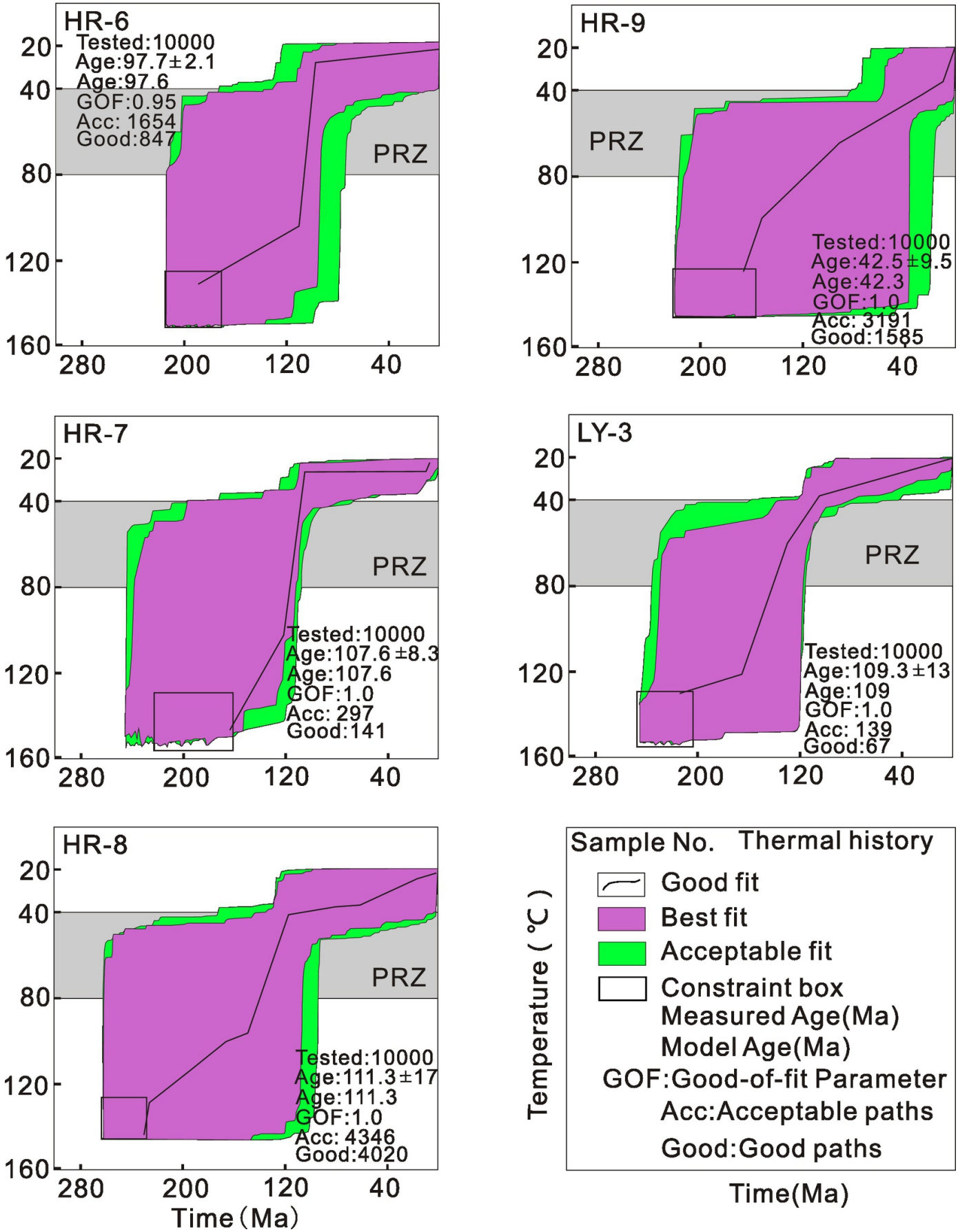
HR-6
Tested:10000
Age:97.7±2.1
Age:97.6
GOF:0.95
Acc: 1654
Good:847
PRZ
HR-9
PRZ
Tested:10000
Age:42.5±9.5
Age:42.3
GOF:1.0
Acc: 3191
Good:1585
HR-7
PRZ
Tested:10000
Age:107.6±8.3
Age:107.6
GOF:1.0
Acc: 297
Good:141
LY-3
PRZ
Tested:10000
Age:109.3±13
Age:109
GOF:1.0
Acc: 139
Good:67
HR-8
PRZ
Tested:10000
Age:111.3±17
Age:111.3
GOF:1.0
Acc: 4346
Good:4020
20
40
80
120
160
280
200
120
40
Time (Ma)
Sample No. Thermal history
Good fit
Best fit
Acceptable fit
Constraint box
Measured Age(Ma)
Model Age(Ma)
GOF:Good-of-fit Parameter
Acc:Acceptable paths
Good:Good paths
Temperature (°C)
Time(Ma)

Figure 9

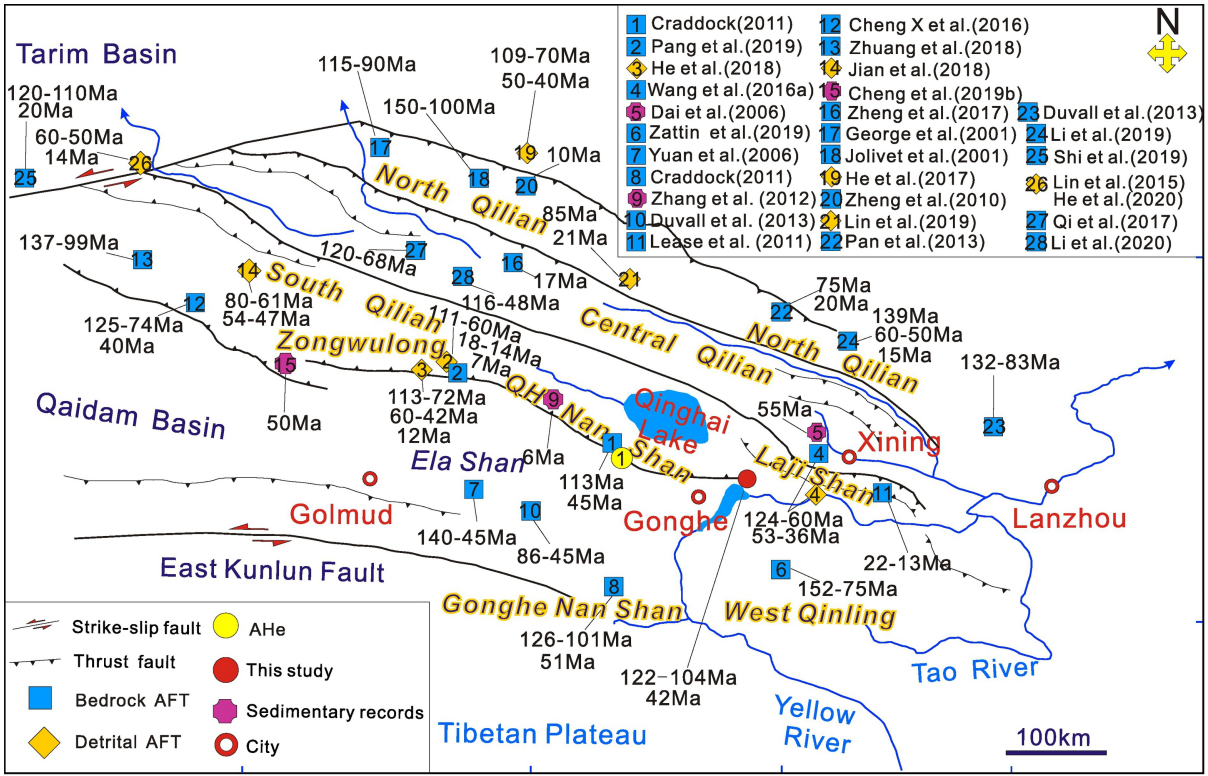
1 Craddock(2011)
2 Pang et al.(2019)
3 He et al.(2018)
4 Wang et al.(2016a)
5 Dai et al.(2006)
6 Zattin et al.(2019)
7 Yuan et al.(2006)
8 Craddock(2011)
9 Zhang et al. (2012)
10 Duvall et al. (2013)
11 Lease et al. (2011)
12 Cheng X et al.(2016)
13 Zhuang et al.(2018)
14 Jian et al.(2018)
15 Cheng et al.(2019b)
16 Zheng et al.(2017)
17 George et al.(2001)
18 Jolivet et al.(2001)
19 He et al.(2017)
20 Zheng et al.(2010)
21 Lin et al.(2019)
22 Pan et al.(2013)
23 Duvall et al.(2013)
24 Li et al.(2019)
25 Shi et al.(2019)
26 Lin et al.(2015) He et al.(2020)
27 Qi et al.(2017)
28 Li et al.(2020)
N
Tarim Basin
120-110Ma
20Ma
60-50Ma
14Ma
115-90Ma
150-100Ma
109-70Ma
50-40Ma
10Ma
North Qilian
85Ma
21Ma
17Ma
116-48Ma
120-68Ma
137-99Ma
South Qilian
80-61Ma
54-47Ma
125-74Ma
40Ma
Zongwulong
111-60Ma
18-14Ma
7Ma
113-72Ma
60-42Ma
12Ma
50Ma
Central Qilian
North Qilian
75Ma
20Ma
139Ma
60-50Ma
15Ma
132-83Ma
55Ma
Qaidam Basin
QHNS
Qinghai Lake
Ela Shan
6Ma
113Ma
45Ma
Laji Shan
Xining
Golmud
140-45Ma
86-45Ma
Gonghe
124-60Ma
53-36Ma
Lanzhou
22-13Ma
East Kunlun Fault
152-75Ma
Gonghe Nan Shan
West Qinling
126-101Ma
51Ma
122-104Ma
42Ma
Tao River
Yellow River
Tibetan Plateau
100km
Strike-slip fault
Thrust fault
Bedrock AFT
Detrital AFT
AHe
This study
Sedimentary records
City
40°N
35°N
90°E
95°E
100°E
105°E

Figure 10